

Domain Walls in Topological Tri-hinge Matter

L. B. Drissi^{1,2,3,*} and E. H. Saidi^{1,2,3}

1-LPHE, Modeling & Simulations, Faculty of Science,

Mohammed V University in Rabat, MB 1014 RP, Rabat, Morocco

2- CPM, Centre of Physics and Mathematics, Faculty of Science, Mohammed V University in Rabat, Morocco

3- Hassan II Academy of Science and Technology, Rabat, Morocco

* E-mails of corresponding author: lalla-btissam.drissi@um5.ac.ma, b.drissi@academiesciences.ma

June 27, 2022

Abstract

Using a link between graph theory and the geometry hosting higher order topological matter, we fill part of the missing results in the engineering of domain walls supporting gapless states for systems with three vertical hinges. The skeleton matrices which house the particle states responsible for the physical properties are classified by the Euler characteristic into three sets with topological index $\chi = 0, 1, 2$. A tri-hinge hamiltonian model invariant under the composite M_1T , M_2T , M_3T is built. In this framework, T is the time reversing symmetry obeying $T^2 = -I$ and the M_i 's are the generators of the three reflections of the dihedral \mathbb{D}_3 symmetry of triangle. To capture the tri-hinge states, candidate materials are suggested, thus opening up a variety of possibilities for investigating and designing robust materials against disorder and deformation.

Keywords: Higher order topological phase; Graph theory; Tri-Hinge matter; Stacked trigonal and hexagonal systems.

1 Introduction

The discovery of topological insulators and superconductors renders the bulk-boundary correspondence a general concept valid for a wider set topological phases of matter; part of which is classified by the periodic Altland-Zirnbauer (AZ) table [1–3]. In this classification, the ten AZ symmetry classes (AZ matter below) are generated by the combination of three internal discrete symmetries, namely the time-reversal (generated by the operator T), the charge conjugation (P), and the chiral symmetry (C) [4–6]. Since this breakthrough, the concept of nontrivial topological band structures has been extended to materials in which other symmetries are also used to protect the topological phases of matter. This includes discrete translation symmetry of the crystal lattice, and other crystalline symmetries like rotations and mirrors protecting gapless boundary states [7–9].

Recently, a new family of topological phase of matter [10, 11] extending the conventional $D/(D - 1)$, sometimes termed as $D/(D - d)$ correspondence with codimension d bigger than 1, is characterized by gapless states in codimension d boundary stabilized by a discrete symmetry \mathbf{g} beyond the AZ invariance generated by \mathbf{T} , \mathbf{P} and \mathbf{C} . In this higher order topological phase (HOT below), the conventional AZ matter appears just as the topological phase associated with codimension one ($d = 1$). As such, HOT phase in 2D matter has topologically protected gapless states at corners of 2D polygonal matter; the particle states on the surface and along the boundary edges are gapped. For the case of HOT matter in 3D, we have two possible locations of the topologically protected states; either on hinges or at corners. Based on this image, attempts have been made so far to classify HOT phases of matter by extending methods used in rederiving AZ table; and also by using other approaches, like the boundary- based approach of [14], bulk perspectives as in [15] and algebraic methods considered in [16].

From the theoretical modeling view point, the D- geometry (skeleton matrix) hosting HOT matter is somehow irregular; and remarkably, it can be thought of in terms of D- dimensional graphs with gapless modes located at the intersection of faces or edges. This is our observation that we want to develop here to complete missing results in literature; in particular in systems with an odd number of hinges and corners. But before commenting this lack of results; notice that the correspondence HOT matter/graphs can be illustrated on several examples [17–23]; for instance in 2D matter with square shape, HOT states live at the four corners where the four edges of the 2D graph intersect. In this case, the gapless states and the domain walls that host them can be interpreted in terms of the well known Jackiw-Rossi state [24] living at vertices of the graph. Notice also that the four corners are related to each other by a cyclic \mathbb{Z}_4 symmetry which plays together with TRS \mathbf{T} a crucial role in the hamiltonian modeling of HOT matter. Likewise for 3D matter having a cubic shape, the gapless states emerging at the 8 corners of the 3D graph lie on the domain walls separating different topological phases. It's the same thing again for 3D cylindrical matter with a square cross section and infinite z direction (no corner), here HOT states live on hinges; and, as we will show in this study, one can still talk about a 3D graph representation although here we have to do with infinite faces. In all the examples given above and also for close cousin geometries, the number of edges and corners where HOT states may live is a multiple of four ($n = 4r$), while for different shape of matter such as the ones with three edges and three corners ($n = 3$), the situation is obscure; to our knowledge no explicit hamiltonian model for HOT matter with three hinges has been built so far due to the difficulty in the engineering of domain walls hosting gapless states. A careful inspection of poly-edge systems reveals that similar results to the above mentioned square, cube and cylinder can only be written down for those regular 2D polygons with $4r$ corners and those regular 3D polyhedrons with $4r$ edges and $4r$ corners; this is partially due to specific properties of \mathbf{C}_{4r}^z generators.

In this paper, we contribute to HOT matter in 3D by filling part of missing results in the engineering of

domain walls supporting gapless states for the family of those matter systems with geometric shapes having three vertical hinges. Physically, this concerns 3D materials with three and six bulk atoms- bondings which allow geometries having three hinges shapes. Theoretically, this family of 3D materials is modeled by a cylindrical matter system with triangular section and boundary surface \mathcal{S} made of three intersecting faces \mathcal{S}_i with different unit normals \mathbf{n}_i ; but vanishing sum $\mathbf{n}_1 + \mathbf{n}_2 + \mathbf{n}_3 = 0$. HOT phases in this family of materials sit either at corners or along hinges; to describe them, we use our observation relating HOT matter to graph theory and then to the Euler characteristic class χ ; so the D- geometry of cylindrical matter is thought of in terms of a 3D graph which turn out to be of three types classified by $\chi = 0, 1, 2$. In this graph classification, corners fall in the classes with $\chi \neq 0$ while cylinders infinite in z-direction belong to the class $\chi = 0$. This classification which will be studied in present paper for tri-hinge systems holds also for other shapes of cylindrical matter including those considered in [10, 11]. Using results on graphs and Dihedral symmetry of triangle, we study the engineering tri-hinge gapless states by using domain wall approach; we found that hamiltonians that solve tri-hinge HOT matter constraints have two kinds of symmetries namely \mathbf{MT} for isosceles triangle and $\mathbf{M}_1\mathbf{T}$, $\mathbf{M}_2\mathbf{T}$, $\mathbf{M}_3\mathbf{T}$ for equilateral triangle; the \mathbf{M} refers to a mirror symmetry; it generates a group \mathbb{Z}_2 .

The presentation is as follows: In section II, we start by introducing tri-hinge matter systems and describe briefly some potential materials that realise them; their bulk atoms have either three bondings or six ones. Then, we study the link between tri-hinge systems and 3D graphs; this relationship is presented through illustrating examples used later on. In section III, we set the basis of hamiltonian modeling of tri-hinge HOT matter; and in section IV, we develop a hamiltonian model for the class $\chi = 0$ and composite $\mathbf{M}_1\mathbf{T}$, $\mathbf{M}_2\mathbf{T}$, $\mathbf{M}_3\mathbf{T}$ symmetries. In the appendix section, we give useful relations concerning the subgroups of the dihedral symmetry of equilateral triangle (Appendix A); then we describe the hexagonal frame used in our calculations; other relations are also developed there (Appendix B); and finally, we give a discussion on the properties of deformation operators according to \mathbf{MT} charges; that is whether they preserve \mathbf{MT} symmetry or they break it (Appendix C).

2 Tri-hinges and graph theory

In this section, we use results on graph theory to approach geometric and topological properties of cylindrical matter with three hinges. We first introduce tri-hinge systems as stacked layers 2D atomic thin materials with hexagonal and triangular structures. Then, we study useful geometric aspects of cylindrical systems as imagined by the schematic pictures of the **Figure 1**. Next, we turn to study their topological properties; here, we think of the cylinder with three hinges as a 3D graph hosting the particle states, and use Euler characteristic χ to classify the 3D cylindrical graphs into three topological classes.

2.1 Tri-hinge systems

Our starting premise is existing or synthetic multilayered structures (MLS) which result from the re-assembly of 2D atomic thin materials through mechanical stacking in one of the three crystallographic directions. MLS have been developed as a good alternative to avoid issues limiting the application of free standing monolayers, such as the strong dependence of the intrinsic behaviors of these single-layer materials on strain and substrate. Thus, the stacking of 2D sheets offers an intriguing perspective of new devices combining exotic phenomena and exploiting the rich physics involved in their constituents as well as the symmetry of their geometry [25–30].

Among the key parameters for the engineering of the structures composing MLS is the large possibility in the choice of potential 2D monolayers that are classified in terms of their elementary bonding states and structures. In this regard, hexagonal and trigonal materials provide a wide range of basic building blocks with unique physical properties which do not exist in their bulk analogs. Graphene is the star member of the honeycomb lattices family exhibiting ultrathin thickness and characterized by intriguing properties [31,32]. Other elements of group-IV, such as silicene, germanene, stanene, and their hybrids, namely SiC, GeC, SnSi, etc, have also emerged to widespread the list of 2D hexagonal materials [33–36]. In parallel, the triangular lattices involve group-III 2D materials like borophene, aluminene and gallene which have only three valence electrons [37–41].

Below we shall think of these MLS as sketched by the two pictures of the **Figure 1**; representing stacked layers of 2D materials having triangular and hexagonal couplings between their in-plane atoms. These

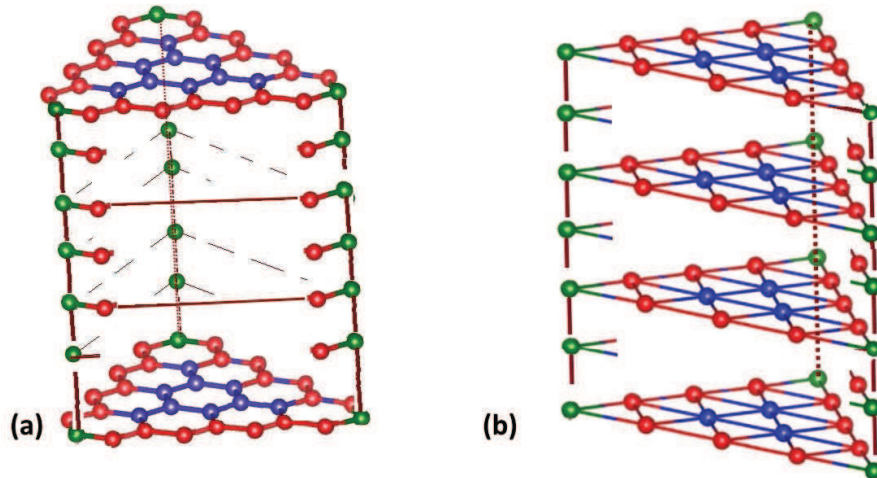


Figure 1: A schematic representation of a cylindrical material with triangular section. Bulk atoms in blue, surface atoms in red and hinge atoms in green. This system is made of an AA stacking of several layers of atoms. Examples of these quasi 2D layers are given by graphene sheets and counterparts like silicene, boron-nitride and hydrides of atoms of column IV. They can also be given by materials like Borophene, Aluminene and homologue having bulk atoms with six bonds.

3D cylindrical materials with open boundaries in transverse directions go beyond the family of cubic and rhombohedral materials because of the difference in the discrete symmetries of their cross sections. Indeed, the cross sections in Fig(1-a) and (1-b) is triangular or hexagonal while in cubic and rhombohedral are given by squares or diamond. Notice that the shape of these sections are known to play an important role in the engineering of higher order topological states; this is because of their discrete symmetries of the cross sections; it is these symmetries that classifies the higher order topological phase of matter [15,42]. For example, the studies of topological phases of cylindrical materials with a square cross section and open boundaries in x- and y- directions [10,11] have revealed that the dihedral symmetry group \mathbb{D}_4 of the transverse square characterises the properties of gapless states of higher order; the symmetry z-axis of order 4 that form the \mathbb{Z}_4 subgroup of \mathbb{D}_4 characterises the chiral gapless hinge states; while mirrors generating \mathbb{Z}_2 subgroups lead to gapless helical states on hinges.

2.2 Cylindrical matter: geometric aspects

Generally speaking, 3D cylindrical matter with several hinges are non regular geometries which can be approached from their boundary properties. The boundary surface of the 3D material is in some sense the main pillar that encodes the geometric properties of the full 3D system. Below, we describe rapidly four constituents that play a crucial role in studying HOT matter and which are related to the boundary surface \mathcal{S} .

1) *the bulk \mathcal{B} with $\mathcal{S} = \partial\mathcal{B}$*

The bulk of the matter system with a boundary $\partial\mathcal{B}$ is parameterised by three variables namely $\mathbf{r} = (x, y, z)$ with values in a given subset of the 3D space; it hosts gapped bulk states $\Psi(\mathbf{r})$ with dynamics governed by an hamiltonian H whose structure will be discussed later on; see Eq(3.1). In the reciprocal space with variables $\mathbf{k} = (k_x, k_y, k_z)$, the gapped bulk states are described by wave functions $\Psi_{\mathbf{k}}^{\pm}$ with positive and negative frequencies; the Ψ^+ for conduction and the Ψ^- for valence bands. These wave functions are solutions of the eigenvalue equation $H_{\mathbf{k}}\Psi_{\mathbf{k}} = E_{\mathbf{k}}\Psi_{\mathbf{k}}$ with non vanishing gap energy

$$E_g(\mathcal{B}) > 0 \tag{2.1}$$

as required by HOT matter. In our analysis, this bulk \mathcal{B} is given by the interior of the cylindrical pictures filled by the blue atoms in x-y plane and along z-axis of the Figures 1. For our modeling, we represent these atomic structures by the cylinders of the Figure 2. The graph in the left is infinite in z-direction; it has no corner, the one in the middle is semi infinite, it has three corners and the graph on the right side is finite and has 6 corners.

2) *the boundary surface \mathcal{S}*

The boundary surface \mathcal{S} contains the bulk \mathcal{B} ; for the pictures of the Figure 2, it is given by a connexion of several intersecting 2D boundary faces \mathcal{S}_i . These faces, thought of below as planar, are parameterised by two independent variables say (u_i, v_i) ; and they play an important role in the

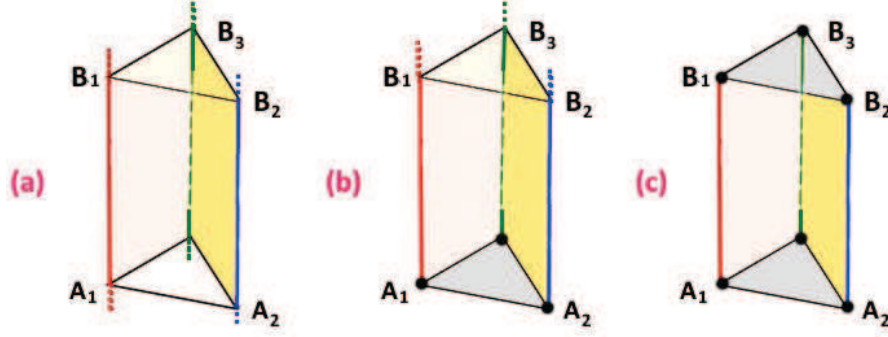


Figure 2: Examples of tri-hinge systems with boundary surfaces S given a connex union of several faces S_i : (a) S is made of three vertical faces and three hinges; the upper and the lower faces are fictitious; they are pushed to $\pm\infty$ or identified by periodicity. (b) S is given by three vertical faces and a horizontal one; the upper face is pushed to $+\infty$. Besides hinges, here we have moreover three vertices represented by black dots. (c) S is made of five faces; three vertical faces and two horizontal ones given by the upper and lower full triangles; here we have six corners.

geometrical characterisation of the tri-hinge systems as they can be used to define all those sub-geometrical objects including hinges and corners. In the example depicted by the third picture of the Figure **2-c**, the connex union of the S_i faces define the full boundary surface of the material and can be heuristically presented as follows

$$\mathcal{S} = \mathcal{S}_1 + \mathcal{S}_2 + \mathcal{S}_3 + \mathcal{S}_4 + \mathcal{S}_5 \quad (2.2)$$

This picture represents a 3D system with full open boundaries and so concerns third order topological phase (TOTIs in language of [12]) with gapless states at corners. For the Figure **2-c**, the boundary surface S is compact and is made of three vertical faces $\mathcal{S}_1, \mathcal{S}_2, \mathcal{S}_3$ and two horizontal ones $\mathcal{S}_4, \mathcal{S}_5$. An example of a vertical face is given by the quadrilateral face $\mathcal{F}_{A_1 A_2}^{B_1 B_2}$ and a horizontal one by the triangular $\mathcal{F}_{A_1 A_2 A_3}$.

In the cylindrical picture **2-a** with z-axis thought as infinite, we have three planar surfaces $\mathcal{S}_1, \mathcal{S}_2, \mathcal{S}_3$ with relative orientation angles $\frac{\pi}{3}$; these surfaces are populated by atoms with red color in the Figure **1**. For HOT matter, surface states have non vanishing gap energy

$$E_g(\mathcal{S}) > 0 \quad (2.3)$$

3) the hinges \mathfrak{h}_{ij}

Hinges \mathfrak{h}_{ij} of the cylindrical systems of the Figure **2** are defined by the intersection of pairs of faces like

$$\mathfrak{h}_{ij} = \mathcal{S}_i \cap \mathcal{S}_j \quad (2.4)$$

For example, the hinge $\mathfrak{h}_{A_1 A_2}$ is given the intersection of the $\mathcal{F}_{A_1 A_2}^{B_1 B_2}$ and $\mathcal{F}_{A_1 A_2 A_3}$ faces. These \mathfrak{h}_{ij} hinges are parameterised by one variable say $w_{ij} \sim z$ and are particularly interesting in the study of

the second order topological phase (SOTIs)

$$E_g(\mathfrak{h}) = 0 \quad (2.5)$$

as gapless states propagate on these lines. In our situation, we have three vertical hinges $\mathfrak{h}_1, \mathfrak{h}_2, \mathfrak{h}_3$ where live atoms with a green color as depicted by the Figure 1.

4) *the corners* \mathfrak{C}_{ijk}

Corners \mathfrak{C}_{ijk} in cylindrical systems are as shown by the pictures (b) and (c) of the Figure 2; they can be defined in two ways; either as the intersection of three faces like $\mathfrak{C}_{ijk} = \mathcal{S}_i \cap \mathcal{S}_j \cap \mathcal{S}_k$; or as the intersection of two hinges like $\mathfrak{h}_{ij} \cap \mathfrak{h}_{jk}$. Corners, where live gapless states and no such states elsewhere, define the third order topological phase.

2.3 Graph representation and topology

Higher topological order phase of 3D systems with three hinges are particular 3D materials with gapless states living either in codimension zero (gapless states at corners); or codimension one (gapless states along hinges). This physical classification brings us to ask a question about the classification of skeleton matrices inhabiting particle states; this issue is addressed below.

2.3.1 Euler characteristic

From an abstract view, matter skeletons are just particular 3D graphs to which we can apply known mathematical results such as the Euler characteristic χ . As such, a classification index of the topological families of 3D cylindrical matter is given by $\chi(\mathcal{S})$, the Euler characteristic of the boundary surface \mathcal{S} of the cylinder with bulk \mathcal{B} . Since we deal with a non conventional boundary surface made of intersecting faces, hinges and corners; the appropriate index to our calculations is given by the following integer number¹

$$\chi(\mathcal{S}) = F - E + V \quad (2.6)$$

where F , E and V refer respectively to the number of faces making \mathcal{S} , the number of its line edges and the number of its point vertices. For an heuristic illustration of this mathematical formula; see the three pictures of the Figure 3. From these pictures, one learns that the empty triangle of the Figure 3-a belongs to the topological class of the circle \mathbb{S}^1 , while the Figures 3-b and 3-c, having $\chi = 1$, belong to the topological class of a half sphere.

With this tool at hand, we can now turn to our systems. Based on the graph representation of the shape of matter systems, we can use the Euler characteristic index (2.6) of graphs to classify the topologies of cylindric materials. In particular, for each \mathcal{S}_i face of Figures 3 corresponds an Euler number equals to unity; that is $\chi(\mathcal{S}_i) = 1$ like the Euler index of a corner that is also equal to 1. The situation is different for hinges that can exist in three types, namely, (i) infinite hinge with no ends; its Euler index is equal to

¹ For any connected planar graph, the Euler characteristic is $F - E + V = 2$. In present study, we work with the relation (2.6) and use it also for non compact surfaces like for the situation where $F = V = 0$.

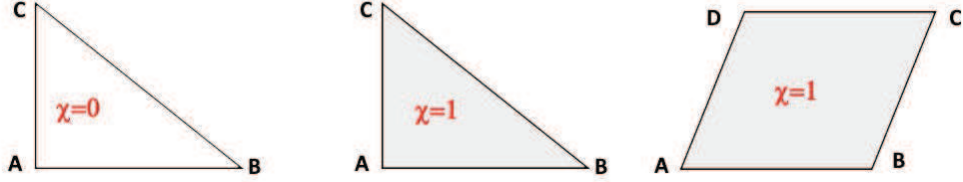


Figure 3: (a) On left an empty triangle with $\chi = 0$. (b) In the middle, a full triangle with $\chi = 1$. (c) On right, a quadrilateral surface with $\chi = 1$. The two last surfaces belong to the same topological class but have different geometries.

$\chi_h = -1$; it is negative; this indicates that the hinge is non compact. (ii) half infinite hinge with one end; its Euler index is equal to $\chi_h = 0$. (iii) finite hinge with two ends; its Euler index is equal to $\chi_h = +1$, it is positive.

2.3.2 Topological classes of graphs

Using eq(2.6), we evaluate the Euler index of the graphs representing the cylindrical matter of the three pictures of the Figure 2. For the Figure 2-c where the boundary \mathcal{S} is fully closed, the numbers (F, E, V) appearing in (2.6) are given by $(5, 9, 6)$, so we have:

$$\chi(\mathcal{S}) = 2 = \chi(\mathbb{S}^2) \quad (2.7)$$

This value teaches us that the Figure 2-c is topologically equivalent to the usual 2-sphere \mathbb{S}^2 which is known to have a χ index equal to 2 as given by the index formula $2 - 2g$ classifying the Riemann surfaces in terms of the number of genus g (the number of handles in the surface) [13]; for the 2-sphere $g = 0$ and for the 2-torus $g = 1$. This means that the boundary surface \mathcal{S} of the Figure 2-c is topologically equivalent to the 2-sphere; in fact the picture 2-c is a particular graph representation of \mathbb{S}^2 given by three quadrilateral planar surfaces and two triangular planar ones; other representations are also possible. In this regards, recall that the geometry of regular 2-sphere can be defined in various but equivalent ways; for example as usual like $X^2 + Y^2 + Z^2 = 1$ from the view of the 3D space; this expression will be used below to introduce a cousin surface to \mathbb{S}^2 namely the real projective surface $\mathbb{R}\mathbb{P}^2$.

Regarding the Figure 2-a, the numbers (F, E, V) are given by $(3, 9, 6)$; they lead to

$$\chi(\mathcal{S}) = 0 = \chi(\mathbb{T}^2) \quad (2.8)$$

This configuration is topologically equivalent of the 2- torus \mathbb{T}^2 with genus $g = 1$; it corresponds physically to the case of a parallelogram in x-y plane as the one given by Figure 3-c; but with parallel borders identified by periodic boundary conditions; for illustration see the Figure 4-a. From this value and the factorisations of \mathbb{T}^2 and its index $\chi(\mathbb{T}^2)$ respectively as the product of two circles $\mathbb{S}^1 \times \mathbb{S}^1$ and the product of their characteristics $\chi(\mathbb{S}^1) \chi(\mathbb{S}^1)$, it follows that cylinders fall as well in the same topological class as the 2-torus. Notice that $\chi(\mathbb{S}^1) = 1 - 1 = 0$, takes the same value as for the empty triangle of the Figure

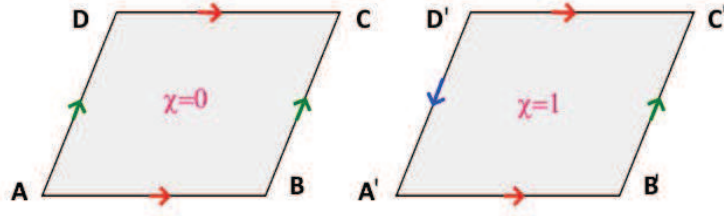


Figure 4: (a) On left the 2-torus where the the parallel edges are identified by periodicity. (b) On right, only the x- edges are identified by periodicity; the y-edges have different orientations.

3-a; this can be interpreted as a deformation of the circle into an empty triangle which is a topological symmetry of the circle.

For the Figure **2-b**, the numbers (F, E, V) are given by $(4, 9, 6)$, so we have

$$\chi(\mathcal{S}) = 1 = \chi(\mathbb{RP}^2) \quad (2.9)$$

revealing that the boundary surface is topologically equivalent to the real projective plane \mathbb{RP}^2 . Recall that the surface \mathbb{RP}^2 is a regular compact surface that can be imagined as close cousin of \mathbb{S}^2 ; it can be defined by starting for the 2-sphere $X^2 + Y^2 + Z^2 = 1$ and demanding the identification of the (X, Y, Z) points with their antipodes $(-X, -Y, -Z)$; roughly, \mathbb{RP}^2 is just an unoriented half sphere; it sits between \mathbb{T}^2 and \mathbb{S}^2 as shown by the pictures of the Figure **2**. Notice that as far as topology is concerned, the value of $\chi(\mathbb{RP}^2)$ is the same as $\chi(D) = 1$, the Euler characteristics of the disc D , and also the same as the full triangular (ABC) and the quadrilateral $(ABCD)$ surfaces of the Figure **3**. These features indicate that although they have different geometric shapes, they belong to the same topological class as \mathbb{RP}^2 and so are topologically equivalent.

Having described the topological aspect of the skeleton matrix hosting matter interpreted here in terms of particular 3D graphs; we now turn to the topological properties of the matter itself.

3 Hamiltonian and domain walls

So far, we have described topological and geometrical properties of tri-hinge cylinder made by gluing three vertical planar surfaces with different orientations. Here, we complete the picture by studying those topological aspects induced by matter itself; that is by properties of quantum states moving in bulk, on the boundary surface and especially the gapless states along hinges of the Figure **2-a**.

3.1 Four bands model

The dynamics of the particle states in 3D cylindrical matter with tri-hinge is implemented by fixing a quantum model with hamiltonian $H = H_{\mathbf{k}}$ that we comment below and develop it further in the next section. For concreteness, we take a tight binding model with hermitian 4×4 hamiltonian matrix describing

2+2 energy bands: 2 for the valence band and 2 for the conducting one; see the Figure 7 for illustration. The general form of this matrix is given by

$$H = \begin{pmatrix} H_{11} & \cdots & H_{41} \\ \vdots & \ddots & \vdots \\ H_{41}^\dagger & \cdots & H_{44} \end{pmatrix} \quad (3.1)$$

it has 16 degrees of freedom H_{mn} which can be approached by expanding it on a 16-dimensional basis T^A like

$$H_{mn} = F_0 \delta_{mn} + \sum_{A=1}^{15} F_A T_{mn}^A \quad (3.2)$$

where F_A 's are functions of momentum \mathbf{k} and also of coupling parameters $\Lambda_1, \dots, \Lambda_r$ defining the model and which we denote collectively by $\mathbf{\Lambda}$. The dependence in momentum is essentially carried by $\sin k_i$ and $\cos k_i$ functions coming from Fourier transforms of bulk wave function. Practical achievements of the above expansion is given by the well known 4×4 gamma matrices $\gamma_1, \gamma_2, \gamma_3, \gamma_4$ and their products; in particular the quadratic, the cubic and the quartic products respectively generated by the typical monomials $\gamma_a \gamma_b$, $\gamma_a \gamma_b \gamma_c$ and $\gamma_a \gamma_b \gamma_c \gamma_d$ with $a < b < c < d$. In terms of the gamma matrices γ_a and their completely antisymmetric product $\gamma_{a_1} \gamma_{a_2} \dots \gamma_{a_i}$ — that are conventionally denoted like $\gamma_{a_1 a_2 \dots a_i}$ with labels as $a_1 < a_2 < \dots < a_i$ —, the 16 degrees of freedom (3.2) are distributed like 1+4+6+4+1 as illustrated on the following table

H_{mn}	\mathbf{I}	γ_a	γ_{ab}	$\gamma_5 \gamma_a$	γ_5
16	1	4	6	4	1

(3.3)

where \mathbf{I} refers to 4×4 identity matrix and where we have also used the properties $\gamma_{abc} \sim \gamma_d \gamma_5 \varepsilon_{abcd}$ and $\gamma_{abcd} \sim \varepsilon_{abcd} \gamma_5$ with ε_{abcd} standing for the completely antisymmetric Levi-Civita tensor in 4d spaces with non zero value $\varepsilon_{1234} = 1$. Regarding these relations, notice that because of the anticommuting property of the gamma matrices often termed as Clifford algebra

$$\gamma_a \gamma_b + \gamma_b \gamma_a = 2\delta_{ab} \quad (3.4)$$

there is only one quartic monomial namely $\gamma_1 \gamma_2 \gamma_3 \gamma_4$; it is precisely the so-called $(-)\gamma_5$ generally used to define chirality of the particle states; this γ_5 anticommutes with the four γ_a 's. Below, we use the following matrix representation of the gamma matrices

$$\gamma_i = \tau_x \sigma_i \quad , \quad \gamma_4 = \tau_y \sigma_0 \quad , \quad \gamma_5 = \tau_z \sigma_0 \quad (3.5)$$

it is given by the tensor product of two sets of Pauli matrices namely σ_i and τ_i with $i = x, y, z$, respectively acting on spin $\uparrow\downarrow$ and orbital degree of freedom ϕ, χ with ϕ referring to conducting band states and χ to the valence ones.

A simple example of the expansion (3.2) is given by the following reduced development

$$H = F_1 \gamma_1 + F_2 \gamma_2 + F_3 \gamma_3 + F_4 \gamma_4 + F_5 \gamma_5 \quad (3.6)$$

This particular hamiltonian is used here below to derive properties encoded in the gap energy E_g . It has only five components $F_a = F_a(\mathbf{k}, \Lambda)$; the others have been set to zero for simplicity; but these zero coefficients might give an interpretation in terms of symmetry requirements on H. Recall that hamiltonians like (3.6) with less F 's or more ones can be classified by using \mathbf{T} , \mathbf{P} and \mathbf{C} of Altland-Zirnbauer as well as extra discrete symmetries like mirrors [15, 42]. Regarding (3.6), notice that the three first coefficients F_i with $i = x, y, z$ are roughly given by sine functions like $F_i = \Delta_i \sin k_i$, which are odd under $\mathbf{k} \rightarrow -\mathbf{k}$, with Δ_i coupling constants interpreted in terms of energy hopping between closed neighboring sites in the material lattice; we often refer to these F_i three terms as kinetic-like. This is because in the limit of small wave vector components around 0 and π , the $\sin k_i$ can be replaced by its linear component $F_i \sim \pm k_i$; and can be presented as a Dirac-like operator $\vec{F} \cdot \vec{\gamma}$. Regarding the two components F_4 and F_5 , they go beyond the x, y, z directions; they are given by adequate combination of cosine functions; for the cubic lattice models they can be imagined as $\Delta_{4/5} + \Delta'_{4/5i} \cos k_i$; they are even under the change $\mathbf{k} \rightarrow -\mathbf{k}$; the $\Delta_{4/5}$ and $\Delta'_{4/5i}$ are extra coupling parameters whose number is fixed by the symmetry of the model. In the limit of small k_i , the cosines can be replaced by ± 1 and so F_4 and F_5 get reduced to constants that are interpreted in terms of mass-like parameters m_4 and m_5 that we comment below; they are functions of the $\Delta_{4/5}$ and $\Delta'_{4/5i}$ coupling parameters.

3.2 Mass parameters and topological states

As for the three $F_i = \sin k_i$ terms, which make it possible to locate the Dirac points in the space of momentum, the m_4 and m_5 mass like parameters play also an important role in dealing with the topological properties captured by gapless states. The m_5 parameter characterises the nature of the topological phases (trivial or not); and the m_4 allows the engineering² of domain walls; the variation of the sign change of m_4 when jumping from a face to its neighboring one indicates existence of a domain wall on which lives a gapless state. To exhibit how the machinery works, we first calculate the spectrum of the hamiltonian of the above four band model; in particular its four energy eigenvalues E_1, E_2, E_3, E_4 . In general this is not a simple task but for eq(3.6), they can be straightforwardly obtained due to (3.4); the energy eigenvalues are not all of them different; they have multiplicity two and are given by $E_{\pm} = \pm \frac{1}{2} E_g$ with

$$E_g = 2\sqrt{F_1^2 + F_2^2 + F_3^2 + F_4^2 + F_5^2} \quad (3.7)$$

referring to the momentum dependent gap energy. This is a function of momentum \mathbf{k} and of the coupling parameters $\mathbf{\Lambda} \equiv (\Lambda_1, \dots, \Lambda_r)$ where r is some positive integer; these parameters are given here by the Δ_i 's, the $\Delta_{4/5}$ and the $\Delta'_{4/5i}$'s. The minimal value of E_g is given by the minima of the five F_a^2 coefficients. In this regards, the minima of the three first $F_i = \sin k_i$ terms are given by $k_{i*} = n_i \pi$; thus leading to a gap energy

$$E_g^{(n_i \pi)} = 2\sqrt{F_4^2|_{n_i \pi} + F_5^2|_{n_i \pi}} \quad (3.8)$$

² The sign of m_4 is important in our construction; it will be used in section 4 for the implementation of domains walls allowing the engineering of topological helical hinge states.

which is a function of the coupling parameters Λ_l of the model; the $F_{4/5}^2|_{n_i\pi}$ refer to $F_{4/5}^2(k_{i*})$ with momentum variables k_i set to k_{i*} . The topological states near $k_{i*} = n_i\pi$ correspond to the situation where $E_g^{(n_i\pi)}$, as functions of the Λ_l 's, vanish at some points $\mathbf{\Lambda}^{(p)}|_{n_i\pi}$ in the coupling parameter space. To shed more light on these gapless states, let us study the case where momentum \mathbf{k} is taken around the Dirac point $(n_x, n_y, n_z) = (0, 0, 0)$; that is a hamiltonian of the form

$$H_D = k_1\gamma_1 + k_2\gamma_2 + k_3\gamma_3 + m_4\gamma_4 + m_5\gamma_5 \quad (3.9)$$

where we have set $\Delta_1 = \Delta_2 = \Delta_3 = 1$. Here, the gap energy is given by $E_g^0 = E_+^0 - E_-^0$, which due to (3.7), is twice $E_+^0(\mathbf{\Lambda})$; so the gapless condition reads as

$$E_g^0(\mathbf{\Lambda}) = 2\sqrt{m_4^2 + m_5^2} = 0 \quad (3.10)$$

and requires two conditions $m_4^2 = 0$ and $m_5^2 = 0$. In the next section, we further develop this study by restricting to tri-hinge systems and develop a way to realise the constraint relations (2.1) and (2.3) as well as the vanishing hinge $E_g(\mathbf{h})$ expressed for this Hamiltonian model by the condition $E_g(\mathbf{\Lambda}) = 0$.

4 Topological hinge states

In this section, we use the results obtained above as well as the triangle symmetries to study the higher topological phase realisations for tri-hinge systems. For that, we have to specify the codimension of the space where live the gapless states as we have two possible locations of these massless- like particles: (i) at the corners which exist for topological graphs with $\chi(\mathcal{S}) \neq 0$; that is for the case of the cylindrical matter bounded on one z-side or on both z-sides as given by the Figures **2-b** and **2-c**. This situation is not addressed in this work because we are interested in the following case: (ii) along the hinges which exist for topological graphs with $\chi(\mathcal{S}) = 0$ as in the case of Figure 2-a which will be studied in the following.

4.1 Triangular section

In this subsection, we use a group theoretical approach to study the constraints imposed by second order topological states in a tri-hinge system. We also give the solution to these constraints for topological tri-hinges using domain walls ideas; and take the opportunity to comment on the results obtained in [10–12] for four-hinge system given by a cylindrical matter with square cross-section. This extra comment may be viewed as an alternative approach to rederive the above mentioned results by using the group theory method.

4.1.1 Group theory approach: case tri-hinge and beyond

Here, we use the group theoretical method to describe symmetry properties of gapless states that propagate along the tri-hinges of the cylindrical matter as depicted by the Figures **1** and the Figure **2-a**. To start, notice that, geometrically, the cylinder with a cross section, given by an equilateral triangular, has z-

direction as a symmetry axis C_3^z of order 3; by threefold order symmetry we mean that $(C_3^z)^3 = I_{id}$ and therefore we have the identity $(C_3^z)^2 = (C_3^z)^{-1}$. In addition to these rotational symmetries, the cylinder of the Fig **2-a** has also three mirror symmetries that we denote like M_1, M_2, M_3 ; these are three reflections obeying the usual property $(M_i)^2 = I_{id}$ and consequently $(M_i)^{-1} = M_i$. So, the cylinder with an equilateral triangular cross section has a total of six symmetries given by

$$I_{id}, C_3^z, (C_3^z)^{-1}, M_1, M_2, M_3 \quad (4.1)$$

The symmetry elements form precisely the so called dihedral symmetry \mathbb{D}_3 of the equilateral triangle; see the appendix A for useful details on this finite discrete group. In this regards, notice that a particularly interesting property of \mathbb{D}_3 is given by its isomorphism with the symmetric group \mathbb{S}_3 acting by permuting the components of a set Σ_3 of three elements, say $\Sigma_3 = \{1, 2, 3\}$; this isomorphism allows to learn many aspects on the \mathbb{D}_3 of the triangle and its representations without having recourse to schematic drawings. Indeed, the permutation group \mathbb{S}_3 has 6 operators realised as follows

$$I_{id}, (123), (132), (12), (23), (31) \quad (4.2)$$

where the three (12), (23) and (31) refer to the transpositions while the two (123) and (132) present the cyclic permutations. By comparing the two above Eq(4.1) and Eq(4.2), we learn that the rotational generator C_3^z can be identified with (123), the inverse $(C_3^z)^{-1}$ with (132) and so on. So the set $\{I_{id}, C_3^z, (C_3^z)^{-1}\}$ is nothing but the subgroup \mathbb{Z}_3 of the dihedral \mathbb{D}_3 ; it is isomorphic to

$$\mathbb{Z}_3 = \{I_{id}, (123), (132)\} \quad (4.3)$$

where I_{id} stands for the identity (1)(2)(3). Before giving other useful symmetry group theoretical details, notice that topologically speaking, the total Euler index χ_{tot} of the graph associated with the cylinder of the Figure **2-a** is equal to zero as described before; this vanishing quantum number can be rederived by computing the total Euler characteristic χ_{tot} given by the sum $\sum_i \chi(\mathcal{S}_i) + \sum_i \chi(\mathfrak{h}_i)$; the first block $\chi(\mathcal{S}_1) + \chi(\mathcal{S}_2) + \chi(\mathcal{S}_3)$ corresponds to the contribution of the three faces which gives $1 + 1 + 1 = 3$; the second block $\sum_i \chi(\mathfrak{h}_i)$ concerns the contribution of the three infinite hinges; it is given by $-1 - 1 - 1 = -3$. So, the total $\chi_{tot} = 3 - 3$ vanishes.

• *domain walls: case tri-hinge*

To engineer gapless states only on the tri-hinges for which the E_g gap energy (3.10) vanishes on \mathfrak{h}_i 's and non zero elsewhere, we use domain walls. In this manner of doing (see also footnote 2), the mass-like term m_4 on either side of the hinge \mathfrak{h}_i is forced to differ in sign putting constraints on the symmetry components of \mathbb{D}_4 . So, the domain walls are characterised by the sign of the mass parameter $m_4 \equiv \mu$ whose absolute value is precisely the gap energy; that is $E_g = |\mu|$. The mass μ changes its sign when we cross the domain wall from left to right and vice versa. As we are looking for gapless states on the hinges, the domain walls are located at the hinges; then the μ changes its signs when going from a given face \mathcal{S}_i to its neighboring faces \mathcal{S}_{i-1} and \mathcal{S}_{i+1} like

$$\begin{aligned} (123) & : \mathcal{S}_1 \rightarrow \mathcal{S}_2 \rightarrow \mathcal{S}_3 \rightarrow \mathcal{S}_1 \\ (132) & : \mathcal{S}_1 \rightarrow \mathcal{S}_3 \rightarrow \mathcal{S}_2 \rightarrow \mathcal{S}_1 \end{aligned} \quad (4.4)$$

where $C_3^z = (123)$ and $(C_3^z)^{-1} = (132)$ are the same as in (4.3). However, for tri-hinge matter, we are faced with a remarkable property concerning 3D systems having an odd number of hinges. As there are three faces, we find that the domain wall picture cannot be fulfilled by sign flip of the mass-like parameter μ while demanding symmetry under \mathbb{Z}_3 . Indeed, as we go from a face \mathcal{S}_i with definite $\text{sgn}(\mu)$; say the face \mathcal{S}_1 with $\text{sgn}(\mu) = +$, and turn around from \mathcal{S}_i toward $\mathcal{S}_{i+3} \equiv \mathcal{S}_i$ by changing $\text{sgn}(\mu)$ whenever we cross from \mathcal{S}_j to the surface \mathcal{S}_{j+1} , we end up with a different sign configuration as shown on the following table

	\mathcal{S}_1	\mathcal{S}_2	\mathcal{S}_3	\mathcal{S}_1	\mathcal{S}_2	\mathcal{S}_3
$\text{sgn}(\mu)$	+	-	+	-	+	-
$\text{sgn}(\mu)$	-	+	-	+	-	+

(4.5)

For the example of an \mathcal{S}_1 with a chosen $\text{sgn}(\mu) = +$ (first row in table (4.5)), one can check that that \mathbb{Z}_3 is no longer a symmetry of the domain wall algorithm; indeed after completing a round tour, the plus sign on \mathcal{S}_1 gets changed into $\text{sgn}(\mu) = -$; but this behavior contradicts the C_3^z symmetry which requires $(C_3^z)^3 = I_{id}$. This indicates that topological phases of tri-hinge domain walls cannot be implemented in terms of rotations; unless we extend the period to two round tours; but this demands higher order rotation axes like C_6^z involving an even number of faces. In this regards, it is interesting to compare this property with a known result in the literature regarding the case of the cylinder considered in [10–12] having four hinges and a square cross section.

- *domain walls: case four-hinge*

A schematic representation of cylindric material with square cross section is depicted by the pictures of the Figure 5. This open cylindric matter has four hinges $\mathfrak{h}'_1, \mathfrak{h}'_2, \mathfrak{h}'_3, \mathfrak{h}'_4$ and four vertical surfaces $\mathcal{S}'_1, \mathcal{S}'_2, \mathcal{S}'_3, \mathcal{S}'_4$

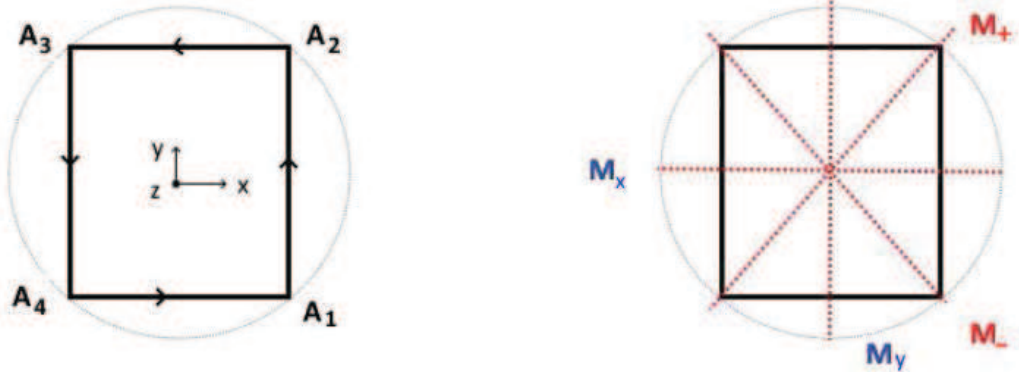


Figure 5: A square cross section with a C_4^z symmetry. On left the four corners (hinges) are related by rotations around z -axis with angles $s\frac{\pi}{4}$ —cyclic \mathbb{Z}_4 symmetry—. On right, the four mirror symmetries; two of them leave invariant two corners and then two hinges.

related among themselves by a four order rotation axis C_4^z and its powers $(C_4^z)^n$ which obey the identities $(C_4^z)^2 = C_2^z$ and $(C_4^z)^3 = (C_4^z)^{-1}$ as it can be checked from the defining group relation $(C_4^z)^4 = I_{id}$; the set of these symmetry operators namely

$$\mathbb{Z}_4 = \{I_{id}, C_4^z, C_2^z, (C_4^z)^{-1}\} \quad (4.6)$$

is a symmetry group of the cylinder with square cross section. For this particular material with square section, the homologue of the table (4.5) is given by

	S'_1	S'_2	S'_3	S'_4	S'_1	S'_2	S'_3	S'_4	
$sgn(\mu')$	+	-	+	-	+	-	+	-	(4.7)
$sgn(\mu')$	-	+	-	+	-	+	-	+	

respecting the \mathbb{Z}_4 symmetry group property $(C_4^z)^4 = I_{id}$. Notice also that for the square cross section, the symmetry group is larger than the above \mathbb{Z}_4 ; the full symmetry of the square is given by the dihedral \mathbb{D}_4 having 8 elements as listed here after

$$I_{id}, \quad C_4^z, \quad C_2^z, \quad (C_4^z)^{-1}, \quad M_x, \quad M_y, \quad M_+, \quad M_- \quad (4.8)$$

This large symmetry group has some remarkable features that make it special for the study of topological states. Contrary to \mathbb{D}_3 of the triangle, the group \mathbb{D}_4 of the square is not isomorphic to the symmetric group \mathbb{S}_4 ; but this is not a problem as there is still an intimate relationship between \mathbb{S}_4 and \mathbb{D}_4 that can be used to perform suitable calculations; the point is that \mathbb{S}_4 has 30 subgroups; three of them are of type \mathbb{D}_4 and nine subgroups of type \mathbb{Z}_2 . In this regards, recall that \mathbb{S}_4 has 24 operators which is bigger than the order 8 of the \mathbb{D}_4 ; the group \mathbb{S}_4 acts by permuting the components of sets Σ_4 of four elements, say $\Sigma_4 = \{1, 2, 3, 4\}$. To fix ideas, the Σ_4 can be imagined in terms of the four corners A_1, A_2, A_3, A_4 of the square as in the Figure 5; they can be also thought of as the four hinges h'_1, h'_2, h'_3, h'_4 of the cylinder; or the four vertical surfaces S'_1, S'_2, S'_3, S'_4 . Regarding the dihedral \mathbb{D}_4 , it is a particular subgroup of \mathbb{S}_4 ; it has two generators for example the 4-cycle (1234) and the transposition (13). Notice moreover, that the dihedral \mathbb{D}_4 itself has in turn subgroups; it has 10 subgroups collected in the following table

subgroups	I_{id}	\mathbb{Z}_2	\mathbb{V}_4	\mathbb{Z}_4	\mathbb{D}_4	
number	1	5	2	1	1	(4.9)

where \mathbb{Z}_p are the usual periodic groups; and where \mathbb{V}_4 stands for the so called Klein group of even transpositions. Notice by the way that the five \mathbb{Z}_2 s are given by the two sets $\{I_{id}, M_x\}$ and $\{I_{id}, M_y\}$; the two \mathbb{Z}_2^\pm given below by Eq(4.10) and $\{I_{id}, C_2^z\}$. What interest us with the table (4.9) is that a careful inspection of the results of [10–12] reveals that it is the subgroups \mathbb{Z}_4 of Eq (4.6) and the two mirror groups

$$\mathbb{Z}_2^+ = \{I_{id}, M_+\} \quad , \quad \mathbb{Z}_2^- = \{I_{id}, M_-\} \quad (4.10)$$

that are behind the engineering of domain walls for cylindrical matter with a square cross section; they preserve the domain wall prescription. The \mathbb{Z}_4 symmetry encodes data on the topological chiral states; while the two \mathbb{Z}_2^\pm s carry information the topological helical states.

- *domain walls: case multi-hinge*

Returning to our tri-hinge system and homologue; and on the light of the above discussion for tri- and four- hinges, we conclude that in general cylindric matter with a polygonal cross section — having an odd

number of hinges, say $2r+1$ — cannot accommodate domain walls as exhibited by the representing table (4.5) for $r=1$. Indeed, a regular polygon with $2r+1$ corner $\{A_1, A_2, \dots, A_{2r+1}\}$ has the dihedral \mathbb{D}_{2r+1} as a symmetry group; this discrete symmetry contains several subgroups among which we have the cyclic \mathbb{Z}_{2r+1} , generated by the $2r+1$ - order rotational axis C_{2r+1}^z , and various \mathbb{Z}_2 mirrors. However, as for the case of the tri-hinge having a \mathbb{Z}_3 symmetry, the \mathbb{Z}_{2r+1} transformations are not compatible with the domain walls algorithm; thus indicating that there no topological chiral states in such cylindric systems; but may have topological helical states. In what follows, we explore the case of helical states in the tri-hinge system; we will show that these topological helical states are indeed protected by mirror reflections M_i of Eq(4.1); but composed with TRS; the mirrors in Eq(4.1) may be viewed as the analogue of the ones in Eq(4.10).

4.1.2 Mirror symmetries in tri-hinge

We begin by noticing that depending on the geometric shape of the triangular section, we distinguish three kinds of tri-hinge cylinders. This classification can be stated in two equivalent manners: (i) In terms of the values of the three corner angles which have to obey $\alpha_1 + \alpha_2 + \alpha_3 = \pi$ and solved in three ways as shown by the second column of the following table,

triangle	corner angles	symmetries	hinge states	protection
scalene	$\alpha_1 \neq \alpha_2 \neq \alpha_3$	I_{id}	gapped	-
isosceles	$\alpha_1 = \alpha_2 \neq \alpha_3$	I_{id}, M	gapless	$\mathbb{Z}_2 T$
equilateral	$\alpha_1 = \alpha_2 = \alpha_3$	I_{id}, M_1, M_2, M_3	gapless	$\mathbb{Z}_2^3 T$

(4.11)

(ii) In terms of the number of plane symmetries (mirror reflections M_i) as given by the third column of the above table and illustrated by the three pictures of the **Figure 6**. In this table we have also given the

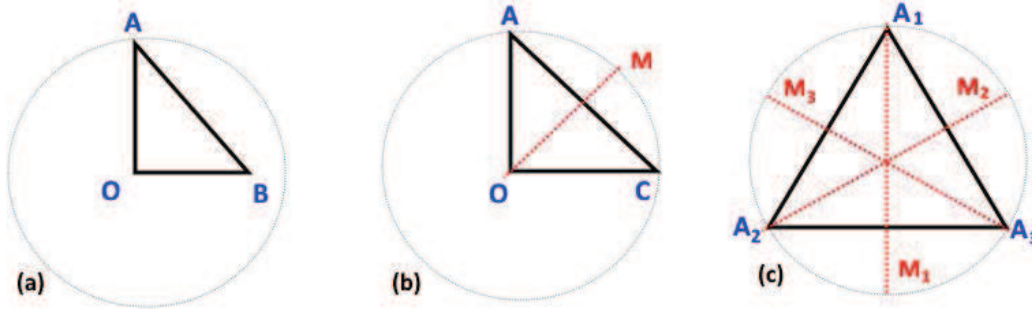


Figure 6: 3D system with triangular cross- sections. (a) Triangle with no reflection symmetry. (b) Isosceles triangle having one reflection symmetry. (c) equilateral triangle having three reflection symmetries.

symmetries that protect the gapless hinge states; these are the $\mathbb{Z}_2 T$ and $\mathbb{Z}_2^3 T$ symmetries of hamiltonian models to be constructed in subsection 4.2.

The classification of the cross sections of the cylindrical matter can be also stated by using symmetry group language. Indeed, the largest symmetry of three objects, say the corners (A_1, A_2, A_3) of an equilateral

triangle —or equivalently the three hinges $(\mathfrak{h}_1, \mathfrak{h}_2, \mathfrak{h}_3)$; or also the faces $(\mathcal{S}_1, \mathcal{S}_2, \mathcal{S}_3)$ — is given by the dihedral \mathbb{D}_3 of the equilateral triangle. This group has 6 elements and it is isomorphic to the \mathbb{S}_3 permutation group whose elements are given by Eq(4.2). From this group theoretical view, it is the equilateral triangle which has the full \mathbb{S}_3 symmetry; the symmetries of the scalene and the isosceles are subgroups of \mathbb{D}_3 ; they are as in table (4.11). For example, the transformation (12) of the **Figure 6-b** leaves the \mathcal{S}_3 face (edge CA) stable and permutes the two other faces \mathcal{S}_1 and \mathcal{S}_2 (edges OC and OA) as follows

$$(12) : (\mathcal{S}_1, \mathcal{S}_2, \mathcal{S}_3) \rightarrow (\mathcal{S}_2, \mathcal{S}_1, \mathcal{S}_3) \quad (4.12)$$

From this algebraic description, we also see that the transformations (4.4) concern the tri-hinge cylinder whose cross section is given by an equilateral triangle. Using these symmetry properties, it becomes clear why that the transformations (123) and (132) are incompatible with domain walls. The reason is that in the engineering of domain walls, we need oriented faces $\mathcal{S}_i^{(+)}$ and $\mathcal{S}_i^{(-)}$ with (\pm) referring to the sign of the mass-like parameter μ . But the permutations (123) and (132) do not know about orientation; they require faces with same orientations; say only $\mathcal{S}_1^{(+)}, \mathcal{S}_2^{(+)}, \mathcal{S}_3^{(+)}$; this intrinsic structure is consequently another manifestation of the absence of topological chiral hinge states in tri-hinge system and generally for an odd number of hinges. Moreover, the need of both $\mathcal{S}_i^{(+)}$ and $\mathcal{S}_i^{(-)}$ is in fact a requirement of topological helical states in tri-hinge; so the engineering of domain walls in tri-hinge demands the doubling of the degrees of freedom in the original hamiltonian model. For instance, the modeling by the 4×4 matrix of Eqs(3.1-3.2) must be extended to an 8×8 ; this construction will be explicitly done in next subsection; it is achieved by introducing a third set of Pauli matrices denoted as $\zeta_x, \zeta_y, \zeta_z$.

In conclusion, the full \mathbb{D}_3 symmetry group of equilateral triangle is incompatible with domain walls' implementation as it breaks the cyclic (123) and its inverse (132). Moreover, knowing that two 3-cycles (123) and (132) belong to the \mathbb{Z}_3 subgroup of \mathbb{D}_3 generated by C_3^z , we end up with the result that it is the \mathbb{Z}_3 subset of \mathbb{D}_3 which is in conflict with the engineering of domain walls in tri-hinge systems. However, the $\mathbb{D}_3 \simeq \mathbb{S}_3$ has other subgroups that may allow domain walls; these are

$$\begin{aligned} \mathbb{Z}_2 & : I_{id} \quad ; \quad (12) = \mathbf{M}_1 \\ \mathbb{Z}'_2 & : I_{id} \quad ; \quad (23) = \mathbf{M}_2 \\ \mathbb{Z}''_2 & : I_{id} \quad ; \quad (31) = \mathbf{M}_3 \end{aligned} \quad (4.13)$$

they correspond to the three mirror reflections depicted by the Figure 6. For later use we set $(ab) = \mathbf{t}_{ab}$; so $\mathbf{M}_1 = \mathbf{t}_{12}$, $\mathbf{M}_2 = \mathbf{t}_{23}$ and $\mathbf{M}_3 = \mathbf{t}_{31}$. In what follows, we show through an explicit construction how these \mathbb{Z}_2 sub-symmetries of \mathbb{D}_3 do have indeed domain walls.

4.2 Domain walls based model

In this subsection, we consider the tri-hinge cylinder given by the Figure 2-a and construct a domain wall's based model that realises the second order topological phase of matter. This model is given by the AII topological class, of the periodic AZ table [1–3], constrained by the \mathbb{Z}_2 mirror symmetries of eqs(4.13). Its

hamiltonian H is not invariant under time reversing symmetry (TRS) T alone, nor under the M_i mirrors alone; it is invariant under the following composed symmetries

$$M_1T \quad , \quad M_2T \quad , \quad M_3T \quad (4.14)$$

To that purpose, we first develop the building method; and turn after to study the implementation of the domain walls and HOT phase in the picture.

4.2.1 Construction method

To build the hamiltonian model of the tri-hinge system with second order topological phase, we start from eq(3.6) and extend its degrees of freedom by adding two ingredients: (i) an extra set of Pauli matrices $\zeta_x, \zeta_y, \zeta_z$ together with the usual identity ζ_0 , this is required by the topological helical states; and (ii) a set of projectors $\varrho_1, \varrho_2, \varrho_3$ given by $\varrho_i = |i\rangle\langle i|$ with $i = 1, 2, 3$; they are in one to one correspondence with the three mirror symmetries M_1, M_2, M_3 . A candidate hamiltonian of the helical tri-hinge model reads as follows

$$H = \mathcal{F}_x \zeta_x \tau_z \sigma_0 + \mathcal{F}_y \zeta_0 \tau_x \sigma_y + \Delta_z (\sin k_z) \varrho \zeta_0 \tau_x \sigma_z + \mathcal{F}_4 \zeta_0 \tau_y \sigma_0 + \mathcal{F}_5 \zeta_z \tau_z \sigma_0 \quad (4.15)$$

Other candidates for H may be written down; they are given by using different choices for the block involving the ζ_i 's; they will be briefly commented in appendix C. As other comments on the above hamiltonian, notice the two following interesting aspects: First, we have five components \mathcal{F}_a to construct; the \mathcal{F}_z has been already replaced by the usual kinetic- like term in reciprocal lattice³ namely $\Delta_z (\sin k_z) \varrho$ where $\varrho = \varrho_1 + \varrho_2 + \varrho_3$; this \mathcal{F}_z is odd under $k_z \rightarrow -k_z$ and commutes with M as required by TRS and mirror symmetry that we take below as $\zeta_0 \tau_0 \sigma_z$; it vanishes for $k_z = n_z \pi$ with $n_z = 0, 1$. So, it remains four \mathcal{F}_a 's to build. Second, we introduced three projectors $\varrho_1, \varrho_2, \varrho_3$; they are needed to implement the three mirror symmetries (4.14); for the proof of this; see eq(4.22) and the comment following it. The \mathcal{F}_a 's we are looking for depend on these projectors; but it turns out that only \mathcal{F}_y which depends on ϱ_i as shown below

$$\begin{aligned} \mathcal{F}_x &= \Delta_x F_x \varrho & , & \quad \mathcal{F}_4 = \Delta_4 F_4 \varrho \\ \mathcal{F}_y &= \Delta_y F_y^i \varrho_i & , & \quad \mathcal{F}_5 = \Delta_5 F_5 \varrho \end{aligned} \quad (4.16)$$

where we have also exhibited the hopping energy parameters Δ_x, Δ_y in x- and y- directions as well as coupling constants Δ_4, Δ_5 . For simplicity, we set below $\Delta_x = \Delta_y = \Delta_z = 1$. From this parametrisation, we see that we have to construct F_x, F_y^i, F_4 and F_5 by using the symmetries (4.14). The calculation of these F_a is very technical; to organize this derivation, we split them into two blocks namely: (1) the $(\mathcal{F}_x, \mathcal{F}_y)$ block which allows to obtain the Dirac points in (k_x, k_y) directions; they will be studied just below. (2) the second block concerns the mass like components $(\mathcal{F}_4, \mathcal{F}_5)$; they are needed to engineer the HOT phase; they will be developed in next sub- subsection; see eqs(4.32)-(4.34).

³ The choice of sin functions is motivated by Dirac theory in small momentum limit. From the real space view, the tight binding hamiltonian, relying of the Figure 1, involves two kinds of creation $\mathbf{a}_\mathbf{r}^\dagger, \mathbf{b}_\mathbf{r}^\dagger$ and annihilation operators $\mathbf{a}_\mathbf{r}, \mathbf{b}_\mathbf{r}$ as in the case of graphene.

- the components $\mathcal{F}_x, \mathcal{F}_y$

To derive the explicit expressions of the components \mathcal{F}_x and \mathcal{F}_y , it is interesting to use the 2D hexagonal coordinate frame; instead of the square coordinates (k_x, k_y) , we use rather the new momentum variables (q_1, q_2, q_3) constrained by the relation

$$q_1 + q_2 + q_3 = 0 \quad (4.17)$$

This parametrisation is interesting as it is invariant under the Dihedral symmetry group \mathbb{D}_3 of equilateral triangle. A particular realisation of these q_i 's is given by thinking of $q_3 = -q_1 - q_2$ and q_1, q_2 as follows

$$q_1 = \frac{k_x + \sqrt{3}k_y}{2}, \quad q_2 = \frac{k_x - \sqrt{3}k_y}{2} \quad (4.18)$$

As far as this choice is concerned, we learn from it that $q_3 = -k_x$; we also learn that the $(12) = t_{12}$ transposition, exchanging q_1 and q_2 , corresponds just to $k_y \rightarrow -k_y$; this property means that \mathcal{F}_y and $\zeta_0 \tau_x \sigma_y$ are both of them odd under the mirror $\mathbf{M} = \zeta_0 \tau_0 \sigma_z$; the oddness of $\mathcal{F}_y(q_1, q_2, q_3)$ under $k_y \rightarrow -k_y$ — or (q_1, q_2) mapped into (q_2, q_1) — is also a requirement of TRS represented by $\mathbf{T} = \zeta_0 \tau_0 \sigma_y \mathbf{K}$; see also appendix C for other properties. The oddness of $\zeta_0 \tau_x \sigma_y$ with respect to \mathbf{M} is manifest due to $\sigma_y \sigma_z = -\sigma_z \sigma_y$. By taking $\mathcal{F}_x(q_1, q_2, q_3)$ and $\mathcal{F}_z(k_z)$ as well as $\mathcal{F}_5(q_1, q_2, q_3)$ to be invariant under $(q_1, q_2) \rightarrow (q_2, q_1)$; it follows that $\zeta_x \tau_z \sigma_0$ and $\zeta_0 \tau_x \sigma_z$ as well as $\zeta_z \tau_z \sigma_0$ should be also invariant under $\mathbf{M} = \zeta_0 \tau_0 \sigma_z$ which is manifest. This realisation is in agreement with the classification obtained in [15] stating that in general we have two representations for \mathbf{M} ; one commuting with TRS and the other one anticommuting with TRS; our \mathbf{M} commutes with \mathbf{T} ; the other is $\zeta_y \tau_y \sigma_y$; it anticommutes with \mathbf{T} .

Regarding the explicit expressions of $\mathcal{F}_x, \mathcal{F}_y$, notice that the constraint $q_1 + q_2 + q_3 = 0$ holds everywhere in our calculations; it can be implemented in the formalism by help of Dirac delta function $\delta_{q_1+q_2+q_3}$; for simplicity of the presentation, we shall hide it. Using the new coordinate frame, we can derive the expressions of the components \mathcal{F}_a as functions of the q_i 's; the explicit calculations are reported in the appendix B; they lead to the two following results: (i) The \mathcal{F}_x is expressed as $F_x \varrho$ with F_x given by $\text{Re } Z$ where the complex $Z = e^{2i\pi q_1} + e^{2i\pi q_2} + e^{2i\pi q_3}$ and its complex adjoint describe transition amplitudes to nearest neighbors. So, F_x reads as follows

$$F_x = \cos(2\pi q_1) + \cos(2\pi q_2) + \cos(2\pi q_3) \quad (4.19)$$

It is invariant under the dihedral \mathbb{D}_3 and vanishes for the values $(q_{1*}, q_{2*}) = (\frac{1}{3}, -\frac{1}{3})$ as well as $(-\frac{1}{3}, \frac{1}{3})$ mod 1; these zeros obey $q_{1*} + q_{2*} = 0$ mod 1. Near, these points, the leading term in the expansion of F_x is given by $\sqrt{3}(\tilde{q}_1 + \tilde{q}_2)/2$ with \tilde{q}_i small deviations. (ii) The component \mathcal{F}_y can be presented as the sum $F_{y1}\varrho_1 + F_{y2}\varrho_2 + F_{y3}\varrho_3$; it involves a triplet (F_{y1}, F_{y2}, F_{y3}) and its explicit expression is a bit laborious; for convenience, it is interesting rewrite it like $\varepsilon_{lij} L_{ij}$ with antisymmetric (triplet) $L_{ij} = L(q_i, q_j)$ as follows

$$\begin{aligned} L_{ij} &= \cos(2\pi q_i) - \cos(2\pi q_j) \\ F_{yl} &= \varepsilon_{lij} [\cos(2\pi q_i) - \cos(2\pi q_j)] \end{aligned} \quad (4.20)$$

The tensor ε_{lij} is the completely antisymmetric Levi-Civita symbol with $\varepsilon_{123} = 1$. Notice the three following features of (4.20): (a) The L_{ij} is odd under the transpositions $(ij) = \mathbf{t}_{ij}$ generating the \mathbb{Z}_2

mirrors of the \mathbb{D}_3 symmetry of the triangle; we have:

$$\mathbf{t}_{ij} : L_{ij} \rightarrow L_{ji} = -L_{ij} \quad (4.21)$$

(b) The antisymmetric matrix L_{ij} is precisely a triplet (L_{12}, L_{23}, L_{31}) transforming as a 3-cycle under the (123) of the \mathbb{Z}_3 subgroup of the \mathbb{D}_3 . This 3-cycle is just the \mathcal{C}_3^z rotation of the cylinder as described in appendix A. It acts on the mirror symmetries as

$$\mathcal{C}_3^z \mathbf{M}_1 = \mathbf{M}_2 \quad , \quad \mathcal{C}_3^z \mathbf{M}_2 = \mathbf{M}_3 \quad , \quad \mathcal{C}_3^z \mathbf{M}_3 = \mathbf{M}_1 \quad (4.22)$$

and teaches us that the realisation of the symmetries eqs(4.14) is equivalent to realising \mathcal{C}_3^z and \mathbf{M}_1 . However, the \mathcal{C}_3^z is realised by the projectors $\varrho_1, \varrho_2, \varrho_3$ as exhibited by eq(6.11) of appendix B; it is this property that is behind the use of the ϱ 's. (c) The set of zeros of the L_{ij} that intersect with those of \mathcal{F}_1 is given by $(q_{1*}, q_{2*}) = \pm(\frac{1}{3}, -\frac{1}{3})$; these zeros give the Dirac points where live the HOT states we are interested in. Near these points, the leading term in the expansion of F_2 is given by $\sqrt{3}(\tilde{q}_1 - \tilde{q}_2)/2$.

To exhibit the symmetries (4.14) of H , it is interesting to put it into a form where the three hinges are apparent. In what follows, we show that H can be put as follows

$$H = \begin{pmatrix} \mathcal{H}(q_1, q_2) & 0 & 0 \\ 0 & \mathcal{H}(q_2, q_3) & 0 \\ 0 & 0 & \mathcal{H}(q_3, q_1) \end{pmatrix} \quad (4.23)$$

where the $\mathcal{H}_{ij} = \mathcal{H}(q_i, q_j)$ describe a hinge hamiltonian invariant under $\mathbf{M}_i \mathbf{T}$. As for L_{ij} , the three $\mathcal{H}_{12}, \mathcal{H}_{23}, \mathcal{H}_{31}$ are related to each other by the permutation cycle (123) generating \mathbb{Z}_3 subsymmetry of \mathbb{D}_3 . To that purpose, we use the relation $\varrho = \varrho_1 + \varrho_2 + \varrho_3$ to decompose the hamiltonian (4.15) as the sum $H_1 \varrho_1 + H_2 \varrho_2 + H_3 \varrho_3$. These H_l 's differ from each other only by the component \mathcal{F}_y ; by substituting $F_{yl} = \varepsilon_{lij} L_{ij}$, and setting $H_l = \varepsilon_{lij} \mathcal{H}_{ij}$, we can put the H_l 's in the equivalent form

$$\mathcal{H}_{ij} = \Delta_x F_x \zeta_0 \tau_x \sigma_x + \Delta_y L_{ij} \zeta_0 \tau_x \sigma_y + \Delta_z (\sin k_z) \varrho \zeta_0 \tau_x \sigma_z + \mathcal{F}_4 \zeta_0 \tau_y \sigma_0 + \mathcal{F}_5 \zeta_z \tau_z \sigma_0 \quad (4.24)$$

where now the \mathcal{H}_{ij} is a function of (q_i, q_j) together with the constraint $q_1 + q_2 + q_3 = 0$; i.e $\mathcal{H}_{ij} = \mathcal{H}(q_i, q_j)$ times the Dirac delta function $\delta_{q_1+q_2+q_3}$. In this \mathcal{H}_{ij} , the components F_x and L_{ij} are respectively given by (4.19) and (4.20); the \mathcal{F}_4 and \mathcal{F}_5 are still missing. If we turn off \mathcal{F}_4 and \mathcal{F}_5 , the reduced $\mathcal{H}_{ij}|$ is invariant under the time reversing symmetry \mathbf{T} represented by $\zeta_0 \tau_0 \sigma_y \mathbf{K}$ and the mirror symmetry \mathbf{t}_{ij} permuting the variables q_i and q_j ; both \mathbf{T} and \mathbf{t}_{ij} leave invariant Dirac delta $\delta_{q_1+q_2+q_3}$. However, by turning on \mathcal{F}_4 and \mathcal{F}_5 , the invariance of \mathcal{H}_{ij} is conditioned by the constraints

$$\begin{aligned} \mathcal{F}_4(-q_i, -q_j, -k_z) &= -\mathcal{F}_4(q_i, q_j, k_z) \\ \mathcal{F}_5(-q_i, -q_j, -k_z) &= +\mathcal{F}_5(q_i, q_j, k_z) \end{aligned} \quad (4.25)$$

required by \mathbf{T} ; and the conditions

$$\begin{aligned} \mathcal{F}_4(q_j, q_i, k_z) &= -\mathcal{F}_4(q_i, q_j, k_z) \\ \mathcal{F}_5(q_j, q_i, k_z) &= +\mathcal{F}_5(q_i, q_j, k_z) \end{aligned} \quad (4.26)$$

demanded by \mathbf{t}_{ij} . A realisation of these constraints gives a tri-hinge model invariant under (4.14). This issue will be studied after commenting the gap energy since it too is dependent on.

- *gap energy*

The energy eigenvalues of \mathcal{H}_{ij} denoted as $E_1^{[ij]}, E_2^{[ij]}, E_3^{[ij]}, E_4^{[ij]}$ are not all of them different; they have multiplicities and can be presented as $E_{\pm}^{[ij]} = \pm 2E_g^{[ij]}$ with gap energy given by

$$E_g^{[ij]} = 2\sqrt{F_1^2 + L_{ij}^2 + \sin^2 k_z + F_4^2 + F_5^2} \quad (4.27)$$

The Dirac points (q_{i*}, q_{j*}, k_{z*}) are obtained by solving $F_x^2 + F_y^2 + \sin^2 k_z = 0$; using previous results, we end up with the four following points modulo periods

$$\left(\frac{1}{3}, -\frac{1}{3}, 0\right), \quad \left(-\frac{1}{3}, \frac{1}{3}, 0\right), \quad \left(\frac{1}{3}, -\frac{1}{3}, \pi\right), \quad \left(-\frac{1}{3}, \frac{1}{3}, \pi\right) \quad (4.28)$$

Notice that under TRS, the point $(\frac{1}{3}, -\frac{1}{3}, 0)$ is not invariant; it transforms into $(-\frac{1}{3}, \frac{1}{3}, 0)$; the same feature holds for $(\frac{1}{3}, -\frac{1}{3}, \pi)$ which is mapped into $(-\frac{1}{3}, \frac{1}{3}, \pi)$. However, the composition TRS with mirror symmetry (i.e: \mathbf{MT}), the Dirac points are invariant as mirror symmetry permutes q_{i*} and q_{j*} and leaves k_{z*} invariant. At these Dirac points, the above energy eigenvalues reduce down to $E_{\pm} = \pm 2E_g$ with

$$E_g = \frac{1}{2}\sqrt{m_4^2 + m_5^2} \quad (4.29)$$

where the mass- like m_4, m_5 are the values of F_4, F_5 at these points. To engineer gapless states on the hinges, we need the explicit expressions of functions F_4 and F_5 .

4.2.2 Implementing domain walls and HOT phase

Here, we construct mass-like functions F_4 and F_5 solving the constraint eqs(4.25-4.26). In our calculations that follow, we shall think of F_5 as the quantity defining the topological phase of the model; and of the F_4 as the quantity defining the domain walls needed by gapless hinge states.

We begin by recalling that in the AII topological class of AZ table, time reversing operator \mathbf{T} obeys $\mathbf{T}^2 = -I_{id}$; it is represented here by the 8×8 matrix operator $\zeta_0 \tau_0 \sigma_y \mathbf{K}$ where \mathbf{K} is the usual complex conjugation and where ζ_i, τ_i and σ_i are three sets of Pauli matrices. This \mathbf{T} operator, whose inverse \mathbf{T}^{-1} is equal to $-\mathbf{T}$, reads in terms the 4×4 gamma matrices used in (3.5) like $\mathbf{T} = i\zeta_0 \gamma_1 \gamma_3 \mathbf{K}$; as such it anticommutes with $\gamma_1, \gamma_2, \gamma_3, \gamma_5$; but commutes with $\gamma_4 = \tau_y \sigma_0$ due to $\mathbf{K} \gamma_4 = -\gamma_4 \mathbf{K}$. It is this last property that allows us to implement domain walls in the construction and then the realisation of a higher order topological phase.

- *Component $\mathcal{F}_4 = \Delta_4 F_4$*

Time reversing symmetry requires $F_4(q_i, q_j)$ to be an odd function under \mathbf{T} ; that is $F_4(-q_i, -q_j) = -F_4(q_i, q_j)$, a behavior that cannot be fulfilled as $F_4(q_i, q_j)$ is made of cosine functions $\cos k_i$ which are even under \mathbf{T} . This difficulty will be effectively counterbalanced by the use of the geometric symmetries of HOT phase given by the mirrors (4.14) as follows

$$(\mathbf{MT}) \mathcal{H}(q_i, q_j, k_z) (\mathbf{MT})^{-1} = \mathcal{H}(-q_j, -q_i, -k_z) \quad (4.30)$$

where (\mathbf{MT}) generates a composed TRS-Mirror symmetry. The reflection operator \mathbf{M} acts on momentum (q_i, q_j) by permuting the variables and on matrices by the representation $\zeta_x \tau_y \sigma_2$ which reads also as $i\zeta_x \gamma_y \gamma_5$; it anticommutes with $\zeta_0 \gamma_y$, commutes with $\zeta_0 \gamma_4, \zeta_z \gamma_5$ and leaves invariant $\delta_{q_1+q_2+q_3}$; so we have

$$\mathbf{M}\mathcal{H}(q_i, q_j, k_z)\mathbf{M} = \mathcal{H}(q_j, q_i, k_z) \quad (4.31)$$

An appropriate solution of F_4 that is independent of momentum k_z along the hinges is given by the factorised expression $f_{41}.f_{42}.f_{43}$ with f_{4i} factors given by

$$\begin{aligned} f_{41} &= \cos 2\pi q_1 - \cos 2\pi q_2 \\ f_{42} &= \cos 2\pi q_2 - \cos 2\pi q_3 \\ f_{43} &= \cos 2\pi q_1 - \cos 2\pi q_3 \end{aligned} \quad (4.32)$$

and $q_1+q_2+q_3 = 0$. Notice that under \mathbf{t}_{12} , the factor f_{41} changes its sign while f_{42} and f_{43} get interchanged; the f_{41} vanishes on the hinge \mathfrak{h}_{12} in agreement with the domain wall prescription. The same feature holds for the transformations under \mathbf{t}_{23} and \mathbf{t}_{31} . By substituting $q_3 = -q_1 - q_2$ and setting $Q_i = 2\pi q_i$, we have

$$F_4 = (\cos Q_1 - \cos Q_2) [\cos Q_2 - \cos(Q_1 + Q_2)] [\cos Q_1 - \cos(Q_1 + Q_2)] \quad (4.33)$$

whose leading term around the Dirac points is $9\sqrt{3}(\tilde{q}_1 - \tilde{q}_2)/8$.

- *Component \mathcal{F}_5*

Regarding the construction of term $\mathcal{F}_5(q_i, q_j, k_z)$, it is even under time reversing symmetry \mathbf{T} and even under the \mathbf{t}_{ij} 's. A candidate is given by

$$\mathcal{F}_5 = \Delta_5 - \frac{\Delta'_{5y}}{2\pi} [\cos 2\pi q_1 + \cos 2\pi q_2 + \cos 2\pi q_3] - \Delta'_{5z} \cos k_z \quad (4.34)$$

where Δ_5, Δ'_{5y} are couplings constants. The structure of this function resembles to the one of a cylinder with a square cross section. Nevertheless, the above F_5 has a special feature. The particularity of this choice of F_5 is that at the Dirac points (q_{1*}, q_{2*}) given by $\pm(\frac{1}{3}, -\frac{1}{3})$, it reduces to $\xi - \cos k_z$ where we have set $\xi = \Delta_5/\Delta'_{5z}$; but this quantity has no dependence into the coupling Δ'_{5y} at all. This may be explained as due to the fact that F_5 can be also presented like

$$\mathcal{F}_5 = \Delta_5 + \Delta'_{5y} \frac{\partial F_y}{\partial q_2} - \Delta'_{5z} \cos k_z \quad (4.35)$$

with $\frac{\partial F_y}{\partial q_2} = -2\pi F_x$ which vanishes identically for (q_1, q_2) equals to $\pm(\frac{1}{3}, -\frac{1}{3})$. Notice also that the reduced expression $\xi - \cos k_z$ has a zero only if $-1 \leq \xi \leq 1$; otherwise there is no gapless state and then no topological insulating phase. Notice moreover that near the Dirac points \mathbf{k}_* given by $(\pm\frac{1}{3}, \mp\frac{1}{3}, n_z\pi)$, we can set momentum $\mathbf{k} \sim \mathbf{k}_* + \delta\mathbf{k}$, and approximate the energy eigenvalues (4.27) in nearby of hinges by the quantities $\pm(\delta^2 + \sin^2 k_z + (\xi - \cos k_z)^2)^{1/2}$. The variation of these reduced energies as a function k_z is depicted in the Figure 7 for some given values of the parameters ξ and δ^2 . In this figure, we see the gapless mode (in red) traversing the bulk band gap.

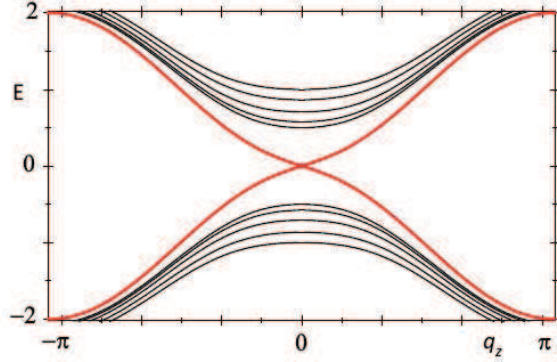


Figure 7: Band energies E_{\pm} as a function of k_z near the Dirac points $(\pm\frac{1}{3}, \mp\frac{1}{3}, 0)$, the parameters are as $\xi = 1$ and $\delta^2 = 0.25, 0.5, 0.75$ and 1 .

5 Conclusion and comments

Higher order topological phase of 2D and 3D matter using domain walls for the engineering of gapless states in codimension zero and one spaces have been extensively studied for materials; especially those having cubic and rhombohedral structures. In this paper, we have contributed to this matter by completing a missing part of the picture by studying those higher order topological phases concerning the family of materials having triangular and hexagonal structures. For this particular tri-hinge systems, the implementation of domain walls has been a major problem towards the theoretical construction of explicit Hamiltonian models describing the higher topological phase. Using the power of the Dihedral symmetry group \mathbb{D}_3 of the triangle and its representations; we have looked for a group theoretical explanation of the difficulty in the insertion of domain walls to protect gapless hinge states in a cylindrical system with cross section given by an equilateral triangle. As a result we have been able to identify two parts in the Dihedral symmetry \mathbb{D}_3 of the triangles. In particular, we found, amongst others, that the \mathbb{Z}_3 subgroup of \mathbb{D}_3 forbids domain walls protecting the chiral hinge states, whilst its three subgroups $\mathbb{Z}_{2(1)}, \mathbb{Z}_{2(2)}, \mathbb{Z}_{2(3)}$ allow those protecting helical states. Guided by these symmetry properties and using the hexagonal frame to deal with the propagation of quantum states, we have constructed an $\mathbf{M}_i\mathbf{T}$ invariant hamiltonian with manifestly symmetric domain walls. Regarding applications, we have suggested 3D systems where such HOT phase can be observed; these materials are given by a cylindrical system with triangular sections made of the stacking, along the z-axis, of layers of 2D-materials with triangular and hexagonal structures. In the resulting stacking sheets, the electronic properties of bulk atoms, forming three and six bonds, resemble more or less those in their hexagonal and triangular multilayered analogs respectively. However, the hinge atoms, with only two bonds, leave an electron quasi free to hop along the hinges direction.

An other interesting finding of this work is the step we have made towards a classification of higher order topological phases in terms of Euler characteristics index χ . Though this classification does not distinguish cylindrical systems with square and triangular sections, it allows however to foresee three types of cylinders

with Euler characteristics 0,1 and 2 depending on the z-limit of the hinges. Similar pictures can be drawn for systems with square cross section.

6 Appendices

We give three appendices A, B and C: Appendix A collects useful relations concerning the \mathbb{D}_3 symmetry of the equilateral triangle. Appendix B describes the hexagonal coordinates system with applications; and Appendix C discusses deformations δH_k preserving MT .

6.1 Appendix A: \mathbb{D}_3 symmetry

In this appendix, we review useful aspects of the symmetries of the triangles (4.11,4.13) by focussing on the example of the equilateral triangle as it has richer symmetries. We describe the relationships between the axial C_3^z of the equilateral triangle cross-section of the Figures 2 and its plane symmetries M_1, M_2, M_3 . The axial C_3^z symmetry of the equilateral triangle is intimately related with the M_i reflections; for example it can be factorised as the intersection of two plane symmetries M_i and M_{i+1} like

$$C_3^z = M_{i+1}M_i \quad , \quad i = 1, 2, 3 \pmod 3 \quad (6.1)$$

where the three M_j 's are precisely the mirror plane depicted by the Figure 6. This factorisation feature can be checked directly by starting from the set of corners of the triangle ordered like (A_{i-1}, A_i, A_{i+1}) ; and perform two successive mirror symmetries: First; apply the plane symmetry M_i fixing A_i and permuting $\{A_{i-1}, A_{i+1}\}$; this mapping gives (A_{i+1}, A_i, A_{i-1}) . Then, act by M_{i+1} fixing A_{i+1} and permuting the others namely $\{A_{i-1}, A_i\}$; this leads to (A_{i+1}, A_{i-1}, A_i) which is nothing but a cyclic C_3^z transformation of (A_{i-1}, A_i, A_{i+1}) . However, the factorisation (6.1) is deeper and deserves a discussion; it has an interesting interpretation in terms of the Dihedral \mathbb{D}_3 having six elements including the order 3 cyclic \mathbb{Z}_3 — rotations by $\frac{2\pi r}{3}$ — and the three reflections M_1, M_2, M_3 ; i.e:

$$\mathbb{D}_3 = \{I_{id}, C_3^z, (C_3^z)^{-1}, M_1, M_2, M_3\} \quad (6.2)$$

Besides itself and identity, this set has four other subgroups; the cyclic \mathbb{Z}_3 given by $\{I_{id}, C_3^z, (C_3^z)^{-1}\}$ with generator C_3^z , and three \mathbb{Z}_2 's given by $\{I_{id}, M_i\}$ and generated by the reflections M_i ,

subgroups	I_{id}	\mathbb{Z}_2	\mathbb{Z}_3	\mathbb{D}_3
number	1	3	1	1

(6.3)

Moreover, as \mathbb{D}_3 is isomorphic to the permutation group \mathbb{S}_3 of three elements; say $\{a, b, c\}$ —for the three corners A_1, A_2, A_3 —, one can write explicitly these elements by using cycles. In this language, C_3^z is viewed as a particular element of \mathbb{S}_3 amongst the $3! = 6$ possible ones; they include two 3-cycles (abc) and (acb) ; three transpositions (ab) , (ac) , (bc) ; and the identity $(a)(b)(c)$. The C_3^z and its inverse $(C_3^z)^{-1}$

are given by the 3-cycle (abc) and its inverse (acb) ; C_3^z generates the \mathbb{Z}_3 subgroup in above table. The three reflections M_1, M_2, M_3 are given by the simple transpositions $(ab), (ac), (bc)$; they generate the three \mathbb{Z}_2 's in (6.3). Recall that the 6 elements of the group \mathbb{S}_3 can be generated by two non commuting transpositions; say (cb) and (ac) ; we have for example

$$(abc) = (cb)(ac) \quad (6.4)$$

which can be compared with (6.1). Notice moreover that being a 3-cycle, the C_3^z permits in turn to relate the M_1, M_2, M_3 planes to each other as follows

$$C_3^z M_i = M_{i+1} \quad \text{with} \quad i = 1, 2, 3 \pmod{3} \quad (6.5)$$

This conjugation property is interesting for our analysis; it shows that it is enough to restrict the study to one of the three mirror symmetries; say M_1 ; in agreement with the observation of [15]; the results for the two others follow by applying the above conjugation relation.

6.2 Appendix B: Hexagonal frame

We begin by noticing that the computation of the components \mathcal{F}_a 's in (4.15) is some how cumbersome when they are expressed in the cubic frame with momentum vector \mathbf{k} decomposed as $k_x \mathbf{e}_x + k_y \mathbf{e}_y + k_z \mathbf{e}_z$. This is because of the triangular symmetry of the tri-hinge cylinder; so it is interesting to take advantage of this property by using a basis vector frame exhibiting this symmetry namely the hexagonal frame [25,30]. In practice, this can be done by first splitting the momentum vector \mathbf{k} (and generally speaking 3- vectors \mathbf{v}), like $\mathbf{k}_{\parallel} + k_z \mathbf{e}_z$ ($\mathbf{v} = \mathbf{v}_{\parallel} + v_z \mathbf{e}_z$); then express the transverse \mathbf{k}_{\parallel} in the hexagonal basis generated by two vectors planar α_1, α_2 as follows $\mathbf{k}_{\parallel} = q_1 \alpha_1 + q_2 \alpha_2$. In the new basis, the momentum components q_1 and q_2 propagate along α_1 and α_2 directions in similar way to k_x, k_y, k_z which propagate in the cubic $\mathbf{e}_x, \mathbf{e}_y, \mathbf{e}_z$ directions; these q- components are obviously functions of the old k_x and k_y with relationships as in eq(4.18). To engineer domain walls and exhibit the composed symmetry MT , we need other tools whose useful ones for our calculus are described here after. First, recall that the hexagonal basis has a metric $K_{ij} = \alpha_i \cdot \alpha_j$ which is different from the usual cubic metric $\delta_{ij} = \mathbf{e}_i \cdot \mathbf{e}_j$; by implementing z-direction, the K reads as

$$K = \begin{pmatrix} \frac{4}{3} & -\frac{2}{3} & 0 \\ -\frac{2}{3} & \frac{4}{3} & 0 \\ 0 & 0 & 1 \end{pmatrix}, \quad K^{-1} = \begin{pmatrix} 1 & \frac{1}{2} & 0 \\ \frac{1}{2} & 1 & 0 \\ 0 & 0 & 1 \end{pmatrix} \quad (6.6)$$

Notice also that, contrary to the cubic \mathbf{e}_i - vector basis, the hexagonal α_i 's are not reflexive vectors in the sense that one needs also their ω_i dual with metric $K_{ij}^{-1} = \omega_i \cdot \omega_j$; the extra ω_i 's are needed to do projections by using the duality property $\alpha_i \cdot \omega_j = \delta_{ij}$; this is not necessary in the cubic frame as we already have $\mathbf{e}_i \cdot \mathbf{e}_j = \delta_{ij}$. A realisation of these α_i 's and ω_i 's in the \mathbf{e}_i -cubic basis is given by

$$\begin{aligned} \alpha_1 &= (1, +\frac{1}{\sqrt{3}}, 0) & , & & \omega_1 &= (\frac{1}{2}, +\frac{\sqrt{3}}{2}, 0) \\ \alpha_2 &= (1, -\frac{1}{\sqrt{3}}, 0) & , & & \omega_2 &= (\frac{1}{2}, -\frac{\sqrt{3}}{2}, 0) \end{aligned} \quad (6.7)$$

having a mirror symmetry; under the reflection $(\mathbf{e}_x, \mathbf{e}_y) \rightarrow (\mathbf{e}_x, -\mathbf{e}_y)$, the vectors of the pair $(\boldsymbol{\alpha}_1, \boldsymbol{\alpha}_2)$ gets transformed into $(\boldsymbol{\alpha}'_1, \boldsymbol{\alpha}'_2) = (\boldsymbol{\alpha}_2, \boldsymbol{\alpha}_1)$; the same thing holds for the dual basis as we also have $(\boldsymbol{\omega}'_1, \boldsymbol{\omega}'_2) = (\boldsymbol{\omega}_2, \boldsymbol{\omega}_1)$. Notice also that (6.7) is not the unique \mathbb{Z}_2 symmetric way to expand \mathbf{k}_\parallel ; there are two other remarkable basis sets that we comment here below considering that they are interesting in the exhibition of the three \mathbb{Z}_2 mirror symmetries (4.14) which act by permuting the basis vector directions [25, 26]. Instead of the pair $(\boldsymbol{\alpha}_1, \boldsymbol{\alpha}_2)$, one can also consider either the pair $(\boldsymbol{\alpha}_1, \boldsymbol{\alpha}_3)$ or the pair $(\boldsymbol{\alpha}_2, \boldsymbol{\alpha}_3)$; the three planar vectors making these three pairs are linked by the relation $\boldsymbol{\alpha}_1 + \boldsymbol{\alpha}_2 + \boldsymbol{\alpha}_3 = 0$ which is invariant under \mathbb{D}_3 . The same thing can be said about $\boldsymbol{\omega}'_i$'s with $\boldsymbol{\omega}_1 + \boldsymbol{\omega}_2 + \boldsymbol{\omega}_3 = 0$.

By using these hexagonal vector bases, we derive useful relations for our study; for instance by expressing momentum \mathbf{k} like $q_1\boldsymbol{\alpha}_1 + q_2\boldsymbol{\alpha}_2 + k_z\mathbf{e}_z$, we discover (4.18) with $q_1 + q_2 + q_3 = 0$. This constraint captures the full \mathbb{D}_3 symmetry of the triangular section; and is inserted in our calculations through the Dirac delta function $\delta_{(f)}$ where we have set $f = q_1 + q_2 + q_3$; for the simplicity of the presentation, we shall hide this delta function. Notice also that under the reflection $(k_x, k_y) \rightarrow (k_x, -k_y)$, the triplet (q_1, q_2, q_3) gets mapped to (q_2, q_1, q_3) . An example of a function with dependence into the three q_i 's is given by the following complex function $Z(q_1, q_2, q_3)$ that turns out to play an important role in our study

$$Z = e^{2i\pi q_1} + e^{2i\pi q_2} + e^{2i\pi q_3} \quad (6.8)$$

Because of the Dirac delta function, we can present this Z in three manners; one of them is given by solving the condition $f = 0$ like $q_3 = -q_1 - q_2$ and put it back into (6.8); another manner is by substituting $q_2 = -q_1 - q_3$. The real part of above complex function Z gives precisely the F_x - component involved in the hamiltonian (4.15). To complete this digression on the tools and the symmetry properties of the F_a 's, notice also that there are two more decompositions: one concerns the gamma matrix vector $\tilde{\gamma}$ and the other regards the way to compute the scalar product $\vec{F} \cdot \tilde{\gamma}$ appearing in (4.15). In the cubic frame, $\tilde{\gamma}$ decomposes as usual like $\gamma_x\tilde{\mathbf{e}}_x + \gamma_y\tilde{\mathbf{e}}_y + \gamma_z\tilde{\mathbf{e}}_z$ and so the scalar $\vec{F} \cdot \tilde{\gamma}$ can be expanded as $F_x\gamma_x + F_y\gamma_y + F_z\gamma_z$. Here also it is useful to decompose the vectors \vec{F} and $\tilde{\gamma}$ in the hexagonal bases; first, we split the vector operator $\tilde{\gamma}$ like the sum $\tilde{\gamma}_\parallel + \gamma_z\tilde{\mathbf{e}}_z$ and then decompose the transverse $\tilde{\gamma}_\parallel$ as follows $\Gamma_1\tilde{\boldsymbol{\omega}}_1 + \Gamma_2\tilde{\boldsymbol{\omega}}_2$ where the new matrices Γ_1, Γ_2 are linear combinations of the old gamma matrices γ_x, γ_y . Regarding \vec{F} , it is convenient to decompose in same manner as we have done for momentum vector namely like $G_1\tilde{\boldsymbol{\alpha}}_1 + G_2\tilde{\boldsymbol{\alpha}}_2 + k_z\tilde{\mathbf{e}}_z$ where the new G_1, G_2 are functions of F_x, F_y . To compute the various coefficients, we use the projections $G_i = \vec{F} \cdot \tilde{\boldsymbol{\omega}}_i$ and $\Gamma_i = \tilde{\gamma} \cdot \tilde{\boldsymbol{\alpha}}_i$, that when put back into (4.15), we obtain

$$H = G_1\Gamma_1 + G_2\Gamma_2 + \Delta_z(\sin k_z)\gamma_z + F_4\gamma_4 + F_5\gamma_5 \quad (6.9)$$

The block $G_1\Gamma_1 + G_2\Gamma_2$ is obviously equal to $F_x\gamma_x + F_y\gamma_y$ as the scalar product of vectors is frame independent.

In the end of this appendix, notice that the ϱ_i projectors used in section 5 are given by $|i\rangle\langle i|$; their matrix

forms are

$$\varrho_1 = \begin{pmatrix} 1 & 0 & 0 \\ 0 & 0 & 0 \\ 0 & 0 & 0 \end{pmatrix}, \quad \varrho_2 = \begin{pmatrix} 0 & 0 & 0 \\ 0 & 1 & 0 \\ 0 & 0 & 0 \end{pmatrix}, \quad \varrho_3 = \begin{pmatrix} 0 & 0 & 0 \\ 0 & 0 & 0 \\ 0 & 0 & 1 \end{pmatrix} \quad (6.10)$$

and they transform under the \mathbb{D}_3 transformations as collected in the following table

	ϱ_1	ϱ_2	ϱ_3	ϱ_0
$M_1 = t_{12} = (12)$	ϱ_2	ϱ_1	ϱ_3	ϱ_0
$M_2 = t_{23} = (23)$	ϱ_1	ϱ_3	ϱ_2	ϱ_0
$M_3 = t_{31} = (31)$	ϱ_3	ϱ_2	ϱ_1	ϱ_0
$C_3^z = (123)$	ϱ_2	ϱ_3	ϱ_1	ϱ_0

(6.11)

6.3 Appendix C: Deformations preserving MT

In this appendix, we start from the eight band model hamiltonian $H = H_{\mathbf{k}}$ given by Eq(4.15) preserving MT ; and we make comments regarding its deformations $\delta H_{\mathbf{k}}$ due to external fields. We show that there are 59 operators generating $\delta H_{\mathbf{k}}$, part of them preserves MT and the other part breaks MT ; their number depend on intrinsic data of $\delta H_{\mathbf{k}}$. Before going into details, we would like to notice that a complete theoretical description of the deformations of $H_{\mathbf{k}}$ requires involved tools on the algebra of 8×8 Dirac gamma matrices as they encode the information the $\delta H_{\mathbf{k}}$ deviations of $H_{\mathbf{k}}$; they need also to specify the magnitudes of the coupling parameters in the tight binding model (TBM) relying on the stacked lattices depicted by the Figure 1. Below, we will avoid complexity and focus mainly on describing the method and commenting results. To that purpose, we first describe some aspects of $H_{\mathbf{k}}$; then we turn to study the deviations $\delta H_{\mathbf{k}}$, due to perturbations, and the first step towards their full classifications according to their charges under MT ; i.e whether $H_{\mathbf{k}}$ preserves MT or not. For later use, we also recall that the TRS generator T is given by $\zeta_0 \tau_0 \sigma_y \mathbf{K}$ while the mirror M has been realised as $\zeta_0 \tau_0 \sigma_z$; so $MT = i \zeta_0 \tau_0 \sigma_x \mathbf{K}$.

- *Some useful properties of $H_{\mathbf{k}}$*

We start by recalling that the $H_{\mathbf{k}}$ of Eq(4.15) is a hermitian 8×8 matrix having some special properties that are useful for the study of its deformations $\delta H_{\mathbf{k}}$ as well as their protection symmetries. We describe in what follows four of these properties while aiming for $\delta H_{\mathbf{k}}$ and its invariance: (1) The $H_{\mathbf{k}}$ we considered involves 5 terms which may be imagined as given by the following formal sum

$$H_{\mathbf{k}} = \mathcal{F}_1 \mathbf{X}_1 + \mathcal{F}_2 \mathbf{X}_2 + \mathcal{F}_3 \mathbf{X}_3 + \mathcal{F}_4 \mathbf{X}_4 + \mathcal{F}_5 \mathbf{X}_5 \quad (6.12)$$

where the $\mathcal{F}'_i = \mathcal{F}_i(\mathbf{k}, \Lambda)$ are real functions of momentum \mathbf{k} and the hopping parameters Λ as in Eq(4.15).

(2) The \mathbf{X}_i 's are five hermitian 8×8 matrices which are realised in terms of tensor products of three sets of Pauli matrices as $\zeta_\alpha \tau_\alpha \sigma_i$; these products are collected in the following table⁴

generators	\mathbf{X}_1	\mathbf{X}_2	\mathbf{X}_3	\mathbf{X}_4	\mathbf{X}_5
a realisation	$\zeta_x \tau_z \sigma_0$	$\zeta_0 \tau_x \sigma_y$	$\zeta_0 \tau_x \sigma_z$	$\zeta_0 \tau_y \sigma_0$	$\zeta_z \tau_z \sigma_0$

(6.13)

⁴ Along with these 5 matrices $\mathbf{X}_1, \mathbf{X}_2, \dots, \mathbf{X}_5$, we have moreover two other particular matrices: a sixth $\mathbf{X}_6 = \zeta_x \tau_z \sigma_0$ and a seventh $\mathbf{X}_7 = \zeta_y \tau_z \sigma_0$; these matrices haven't been used in Eq(4.15). Notice also that we have $\mathbf{X}_7 = i \mathbf{X}_1 \mathbf{X}_2 \mathbf{X}_3 \mathbf{X}_4 \mathbf{X}_5 \mathbf{X}_6$.

from which we learn that $\mathbf{X}_1, \mathbf{X}_3, \mathbf{X}_5$ are real (even under \mathbf{K}) whilst $\mathbf{X}_2, \mathbf{X}_4$ are imaginary (odd under \mathbf{K}). Notice that the table (6.13) is not complete as there are 59 other 8×8 matrix generators which do not figure in it; and which could be added to Eq(6.12); they will be described later on as they are precisely the generators of $\delta H_{\mathbf{k}}$. (3) Generally speaking, we do not need an explicit realisation of the \mathbf{X}_i 's as in above table; all we need to know is their algebraic properties which are given by: (i) the Clifford algebra reading as $\mathbf{X}_A \mathbf{X}_B + \mathbf{X}_B \mathbf{X}_A = 2\delta_{AB}$ with $A, B = 1, \dots, 6$; (ii) the properties of the \mathbf{X}_A 's under complex conjugation operator \mathbf{K} as it appears in TRS transformations; and (iii) for chiral models, we also need their properties under the operator $\mathbf{X}_7 = i\mathbf{X}_1\mathbf{X}_2\mathbf{X}_3\mathbf{X}_4\mathbf{X}_5\mathbf{X}_6$. These aspects can be learnt from the domain walls prescription of our tri-hinge system requiring the following charges under TRS, mirror \mathbf{M} and their composition \mathbf{MT}

factors	$\mathcal{F}_1\mathbf{X}_1$	$\mathcal{F}_2\mathbf{X}_2$	$\mathcal{F}_3\mathbf{X}_3$	$\mathcal{F}_4\mathbf{X}_4$	$\mathcal{F}_5\mathbf{X}_5$
\mathbf{T}	+	+	+	-	+
\mathbf{M}	+	+	+	-	+
\mathbf{MT}	+	+	+	+	+

(6.14)

From this domain walls prescription as well as the trigonal symmetries of the materials discussed in the heart of the paper requiring particular T- and M- charges for the \mathcal{F}_A coefficients under TRS and mirror \mathbf{M} , we can re-work out the realisation of \mathbf{T} and \mathbf{M} . For later use, we denote the T-charge of the pair $(\mathcal{F}_i, \mathbf{X}_i)$ under TRS as $(q_i, p_i)_T$ so that the T- charge of the product $\mathcal{F}_i\mathbf{X}_i$ is given by $q_{iT} \times p_{iT}$. Similarly, we denote by $(q_i, p_i)_M$ the M- charge of the pair $(\mathcal{F}_i, \mathbf{X}_i)$ under \mathbf{M} so that the M-charge of the monomials $\mathcal{F}_i\mathbf{X}_i$ is given by $q_{iM} \times p_{iM}$. Therefore, the charge of $\mathcal{F}_i\mathbf{X}_i$ under the composite \mathbf{MT} is given by $q_{iT} \times q_{iM} \times p_{iT} \times p_{iM}$. These T- and M- charges are collected in the following table

factors	$(\mathcal{F}_1, \mathbf{X}_1)$	$(\mathcal{F}_2, \mathbf{X}_2)$	$(\mathcal{F}_3, \mathbf{X}_3)$	$(\mathcal{F}_4, \mathbf{X}_4)$	$(\mathcal{F}_5, \mathbf{X}_5)$
T- charge	$(+, +)_T$	$(-, -)_T$	$(-, -)_T$	$(+, -)_T$	$(+, +)_T$
M- charge	$(+, +)_M$	$(-, -)_M$	$(+, +)_M$	$(-, +)_M$	$(+, +)_M$
M- charge	$(+, +)_{MT}$	$(+, +)_{MT}$	$(-, -)_{MT}$	$(-, -)_{MT}$	$(+, +)_{MT}$

(6.15)

from which we learn

$$\mathbf{T} = -i\mathbf{X}_3\mathbf{X}_6\mathbf{K} \quad , \quad \mathbf{M} = i\mathbf{X}_2\mathbf{X}_6 \quad , \quad \mathbf{MT} = \mathbf{X}_3\mathbf{X}_2\mathbf{K} \quad (6.16)$$

By substituting the realisation (6.13) back into above quantities, we deduce the expressions of the symmetry generators of section 4 namely $\mathbf{T} = \zeta_0\tau_0\sigma_y\mathbf{K}$ and $\mathbf{M} = \zeta_0\tau_0\sigma_z$ as well as $\mathbf{MT} = i\zeta_0\tau_0\sigma_x\mathbf{K}$. (4) As noticed earlier, the five \mathbf{X}_i 's obey the Clifford algebra $\mathbf{X}_i\mathbf{X}_j + \mathbf{X}_j\mathbf{X}_i = 2\delta_{ij}$; this feature teaches us that $H_{\mathbf{k}}^2 = E_{\mathbf{k}}^2 I_8$ showing that the square of the hamiltonian is proportional to the 8×8 identity matrix I_8 . This property indicates that the eight energy eigenvalues E_1, \dots, E_8 of the hamiltonian are four fold degenerate; i.e two different energies E_{\pm} ; each with multiplicity 4; these energies are given by $E_{\pm} = \pm \frac{1}{2}E_g$ with gap energy $E_g = 2\sqrt{\mathcal{F}_1^2 + \dots + \mathcal{F}_5^2}$. The vanishing properties of this gap has been studied and commented in the core of the paper.

• *Building $\delta H_{\mathbf{k}}$ and describing its properties*

We begin by noticing that the hamiltonian (6.12) modeling the topological helical states is clearly not the general hamiltonian we may write down; this is because Eq(6.12) has only five degrees of freedom $\mathcal{F}_1, \mathcal{F}_2, \mathcal{F}_3, \mathcal{F}_4, \mathcal{F}_5$; while the most general form of a 8×8 hermitian matrix has 64 components as exhibited by the following expansion

$$\begin{aligned} \tilde{H}_{\mathbf{k}} = & \mathcal{F}^0 \mathbf{X}_0 + \sum_{A=1}^6 \left(\mathcal{F}^A \mathbf{X}_A + i \tilde{\mathcal{F}}^A \mathbf{X}_A \mathbf{X}_7 \right) + \sum_{A<B<C=1}^6 \mathcal{G}^{AB} \mathbf{X}_{ABC} \\ & + \sum_{A<B=1}^6 \left(\mathcal{F}^{AB} \mathbf{X}_{AB} + \tilde{\mathcal{F}}^{AB} \mathbf{X}_{AB} \mathbf{X}_7 \right) + \tilde{\mathcal{F}}^0 \mathbf{X}_7 \end{aligned} \quad (6.17)$$

where $\mathbf{X}_0 = I_8$ and where we have set $\mathbf{X}_{AB} = i \mathbf{X}_A \mathbf{X}_B$ and $\mathbf{X}_{ABC} = i \mathbf{X}_A \mathbf{X}_B \mathbf{X}_C$; this basis is a standard basis useful in dealing with Clifford algebra and fermionic wave functions. This decomposition of $\tilde{H}_{\mathbf{k}}$ corresponds to the following partition of the number 64,

generators	I_8	\mathbf{X}_A	\mathbf{X}_{AB}	\mathbf{X}_{ABC}	$\mathbf{X}_{AB} \mathbf{X}_7$	$\mathbf{X}_A \mathbf{X}_7$	\mathbf{X}_7
64	1	6	15	20	15	6	1

(6.18)

Contrary to Eq(6.12), the hamiltonian $\tilde{H}_{\mathbf{k}}$ has in general eight different energy eigenvalues that can be presented like $E_1^{\pm}, E_2^{\pm}, E_3^{\pm}, E_4^{\pm}$; the four E_i^+ stand for the energies of conducting bands while the four E_i^- give the energies of valence bands; the gap energy E_g is given by $E_{\min}^+ - E_{\max}^-$; and then the knowledge of these E_{\min}^+ and E_{\max}^- is of major importance for several issues; in particular the one regarding those small perturbations breaking \mathbf{MT} and their effect on the gap energy. Here, we will not calculate E_{\min}^+ nor E_{\max}^- as they require specifying magnitudes of the coupling constants in TBM; and also solving a somehow complicated eigenvalue problem which, though interesting numerically, is beyond the main objective of the paper.

In summary, we end up this appendix by saying that the hamiltonian Eq(6.12) modeling helical gapless states in tri-hinge system is a candidate hamiltonian having three remarkable properties: (i) \mathbf{MT} protection; (ii) admitting two energy eigenvalues with multiplicity 4; and (iii) a gap energy $E_g = E_{\min}^+ - E_{\max}^-$ which can take a zero value at Dirac points and for some values of the coupling parameters. The general $\tilde{H}_{\mathbf{k}}$ given by (6.17) goes beyond these properties and may be thought of as $H_{\mathbf{k}} + \delta H_{\mathbf{k}}$; that is describing the deviations of $H_{\mathbf{k}}$. So, the $\delta H_{\mathbf{k}}$ is generated by 59 monomial operators as listed by (6.18). Moreover, as for the T- and M- charges (6.15), one can work out a classification of the deformations $\delta H_{\mathbf{k}}$; they depend on the charges of the coefficients $\mathcal{F}^{A_1 \dots A_i}(\mathbf{k}, \Lambda, \dots)$ in the expansion (6.17). This is a technical question which requires a bigger space for an appendix; we hope to return to it in a future occasion. We conclude by noting that the deformations $\delta H_{\mathbf{k}}$ generally lift the energy degeneracy of $H_{\mathbf{k}}$ and the knowledge of the explicit expression of $E_{\min}^+ - E_{\max}^-$ allows to study the properties of the energy gap induced by small perturbations breaking \mathbf{MT} .

Acknowledgement 1: *Professors Lalla Btissam Drissi and El Hassan Saidi would like to acknowledge "Académie Hassan II des Sciences et Techniques-Morocco" for financial support. They also thank Felix*

von Oppen for stimulating discussions. L. B. Drissi acknowledges the Alexander von Humboldt Foundation for financial support via the Georg Forster Research Fellowship for experienced scientists (Ref 3.4 - MAR - 1202992).

References

- [1] A. Altland and M. R. Zirnbauer, Physical Review B 55,1142 (1997).
- [2] A. P. Schnyder, S. Ryu, A. Furusaki, and A. W. W. Ludwig, Physical Review B 78, 195125 (2008).
- [3] C.-K. Chiu, J.C.Y. Teo, A.P. Schnyder, and S. Ryu, Rev. Mod. Phys. 88, 035005 (2016).
- [4] M. Z. Hasan and C. L. Kane, Reviews of Modern Physics 82, 3045 (2010).
- [5] X.-L. Qi and S.-C. Zhang, Rev. Mod. Phys. 83, 1057,(2011).
- [6] C. L. Kane and E. J. Mele, Phys. Rev. Lett. 95, 146802, (2005).
- [7] C.-K. Chiu, J.C.Y. Teo, A.P. Schnyder, and S. Ryu, Rev. Mod. Phys. 88, 035005 (2016).
- [8] L. Fu, C.L. Kane, and E.J. Mele, Phys. Rev. Lett. 98, 106803 (2007).
- [9] L. Fu, Phys. Rev. Lett. 106, 106802 (2011). (2019).
- [10] W. A. Benalcazar, B. A. Bernevig, and T. L. Hughes, Science 357, 61 (2017).
- [11] W. A. Benalcazar, B. A. Bernevig, and T. L. Hughes, Physical Review B 96, 245115 (2017).
- [12] F. Schindler, Z. Wang, M. G. Vergniory, A. M. Cook, A. Murani, S. Sengupta, A. Y. Kasumov, et al., Higher-order topology in bismuth, Nature physics 14, 918 (2018).
- [13] Schlichenmaier M. (2007) Topology of Riemann Surfaces. Theoretical and Mathematical Physics. Springer, Berlin, Heidelberg, DOI https://doi.org/10.1007/978-3-540-71175-9_2,
- [14] E. Khalaf, Phys. Rev. B 97, 205136 (2018).
- [15] J. Langbehn, Y. Peng, L. Trifunovic, F. von Oppen, and P. W. Brouwer, Phys. Rev. Lett. 119, 246401 (2017).
- [16] L. Trifunovic and P. Brouwer, Phys. Rev. X9, 011012 (2019).
- [17] M. Sitte, A. Rosch, E. Altman, and L. Fritz, Phys. Rev. Lett. 108, 126807 (2012).17
- [18] F. Zhang, C. L. Kane, and E. J. Mele, Phys. Rev. Lett. 110, 046404 (2013).
- [19] T. H. Hsieh, H. Lin, J. Liu, W. Duan, A. Bansil, and L. Fu, Nat. Comm. 3, 982 (2012).

- [20] F. Schindler, A. M. Cook, M. G. Vergniory, Z. Wang, S. S. Parkin, B. A. Bernevig, and T. Neupert, *Science Advances* 01, Vol. 4, no. 6, eaat0346 (2018).
- [21] M. Z. Hasan and C. L. Kane, *Rev. Mod. Phys.* 82, 3045 (2010).
- [22] B. A. Bernevig and T. L. Hughes, *Topological Insulators and Topological Superconductors* (Princeton University Press, 2013).
- [23] X.-L. Qi and S.-C. Zhang, *Rev. Mod. Phys.* 83, 1057 (2011).
- [24] R. Jackiw and C. Rebbi, *Phys. Rev. D* 13, 3398 (1976).
- [25] L.B. Drissi, E.H. Saidi and M. Bousmina, *Phys. Rev. D* 84 014504 (2011).
- [26] L. B. Drissi, E.H. Saidi, Dirac Zero Modes in Hyperdiamond Model, *Phys. Rev. D* 84, 014509, (2011).
- [27] G. Fiori, F. Bonaccorso, G. Iannaccone, T. Palacios, D. Neumaier, A. Seabaugh, S.K. Banerjee, L. Colombo, *Nat. Nanotechnol.* 9 (2014) 768–779.
- [28] F.N. Xia, H. Wang, D. Xiao, M. Dubey, A. Ramasubramaniam, *Nat. Photon.* 8 (2014) 899–907.
- [29] L. Wang, I. Meric, P.Y. Huang, Q. Gao, Y. Gao, H. Tran, T. Taniguchi, K. Watanabe, L.M. Campo, D.A. Muller, *Science* 342 (2013) 614–617.
- [30] L. B. Drissi, E.H. Saidi, M. Bousmina, *Nucl.Phys.B*, Volume 829, Issue 3, (2010).
- [31] K.S. Novoselov, A.K. Geim, S.V. Morozov, D. Jiang, Y. Zhang, S.V. Dubonos, I.V. Grigorieva, A.A. Firsov, *Science* 306 (2004) 666–669.
- [32] L. B. Drissi, E. H. Saidi, and M. Bousmina, *J. Math. Phys* 52, (2011) 022306.
- [33] P. Vogt, P.P. De, C. Quaresima, J. Avila, F. Frantzeskakis, M.C. Asensio, A. Resta, B. Ealet, G.L. Lay, *Phys. Rev. Lett.* 108 (2012) 155501.
- [34] L.F. Li, S.Z. Lu, J.B. Pan, Z.H. Qin, Y.Q. Wang, Y.L. Wang, G.Y. Cao, S.X. Du, H.J. Gao, *Adv. Mater.* 26 (2014) 4820–4824.
- [35] F.F. Zhu, W.J. Chen, Y. Xu, C.L. Gao, D.D. Guan, C.H. Liu, D. Qian, S.C. Zhang, J.F. Jia, *Nat. Mater.* 14 (2015) 1020–1025.
- [36] L. B. Drissi, N. B-J. Kanga, S. Lounis, F. Djeflal and S. Haddad, *Journal of Physics: Condensed Matter* 31 (13), (2019) 135702.
- [37] Mannix AJ, Zhou XF, Kiraly B, et al., *Science* 2015;350:1513–6.
- [38] Zhang ZH, Mannix AJ, Hu ZL, et al., *Nano Lett* 2016;16:6622–7.
- [39] C. Kamal, A. Chakrabarti, M. Ezawa, *New J. Phys.* 17 (2015) 083014.

- [40] R. Wu, I. K. Drozdov, S. Eltinge, P. Zahl, S. Ismail-Beigi, I. Božović, A. Gozar, *Nat. Nanotechnol.* 2019, 14, 44.
- [41] M. L. Tao, Y. B. Tu, K. Sun, Y. L. Wang, Z. B. Xie, L. Liu, M. X. Shi, J. Z. Wang, *2D Mater.* 2018, 5, 035009.
- [42] L. B. Drissi, E. H. Saidi, A signature index for third order topological insulators, *J. Phys: Cond. Matt*, (2020).
- [43] L. B. Drissi, E. H. Saidi and M. Bousmina, *Phys. Rev. D* 84 014504 (2011).